

# A Flexible GMRES Solver with Reduced Order Model Enhanced Synthetic Acceleration Preconditioner for Parametric Radiative Transfer Equation

Zhichao Peng

<sup>a</sup>*Department of Mathematics, The Hong Kong University of Science and Technology, Clear Water Bay, Kowloon, Hong Kong, China*

---

## Abstract

Parametric radiative transfer equation (RTE) occurs in multi-query applications such as uncertainty quantification, inverse problems, and sensitivity analysis, which require solving RTE multiple times for a range of parameters. Consequently, efficient iterative solvers are highly desired.

Classical Synthetic Acceleration (SA) preconditioners for RTE build on low order approximations to an ideal kinetic correction equation such as its diffusion limit in Diffusion Synthetic Acceleration (DSA). Their performance depends on the effectiveness of the underlying low order approximation. In addition, they do not leverage low rank structures with respect to the parameters of the parametric problem.

To address these issues, we proposed a ROM-enhanced SA strategy, called ROMSAD, under the Source Iteration framework in Peng (2024). In this paper, we further extend the ROMSAD preconditioner to flexible general minimal residual method (FGMRES). The main new advancement is twofold. First, after identifying the ideal kinetic correction equation within the FGMRES framework, we reformulate it into an equivalent form, allowing us to develop an iterative procedure to construct a ROM for this ideal correction equation without directly solving it. Second, we introduce a greedy algorithm to build the underlying ROM for the ROMSAD preconditioner more efficiently.

Our numerical examples demonstrate that FGMRES with the ROMSAD preconditioner (FGMRES-ROMSAD) is more efficient than GMRES with the right DSA preconditioner. Furthermore, when the underlying ROM in ROMSAD is not highly accurate, FGMRES-ROMSAD exhibits greater robustness compared to Source Iteration accelerated by ROMSAD.

*Keywords:* Parametric radiative transfer equation; Reduced order model; Krylov method; Synthetic Acceleration; Kinetic equation.

---

## 1. Introduction

Radiative transfer equation (RTE) provides models for particle systems in a wide range of applications, e.g., medical imaging [1], remote sensing [2], nuclear engineering [3], and astrophysics [4]. In multi-query engineering or scientific applications, such as design optimization, inverse problems, sensitivity analysis, and uncertainty quantification, RTE is often solved repeatedly within a parametric setting. The parameters for these parametric problems typically originate from the parametrization of material properties, boundary conditions, or geometric configurations. Due to the need for solving the RTE multiple times, efficient numerical solvers for parametric RTE are highly desired.

Among iterative linear solvers for RTE, Source Iteration (SI) and Krylov solvers with Synthetic Acceleration (SA) [5, 6, 7] are widely used. It is well known that vanilla SI may converge arbitrarily slowly [5]. To accelerate its convergence, SA preconditioner introduces a correction to the scalar flux (also known as the macroscopic density). The ideal scalar flux correction, which guarantees the convergence of SI in the next iteration, is

---

*Email address:* pengzhic@ust.hk ( Zhichao Peng )

the integral of an ideal angular flux correction, which is the solution to an ideal kinetic correction equation. However, solving this ideal kinetic correction equation results in almost the same computational costs as directly solving the original problem. Hence, in practice, a computationally cheap low-order approximation to it is employed. Popular choices include the diffusion limit of the kinetic correction equation in Diffusion Synthetic Acceleration (DSA) [8, 9, 10, 11, 12], the variable Eddington factor in Quasi-Diffusion method [13, 14, 15], and the  $S_2$  approximation in S2SA [16]. However, as pointed out in [17, 6], the effectiveness of SI-SA may degenerate for challenging problems, such as those involving material discontinuities. To overcome this degeneration, [6] extends SA preconditioners to Krylov solvers by rewriting the SI-SA as a left preconditioned Richardson iteration for a memory-efficient discrete formulation of the RTE.

Despite the great success and popularity of these classical SA strategies, their effectiveness hinges on the underlying empirical low order approximations. For instance, when the problem is far from its diffusion limit, DSA may lose its efficiency [18]. Moreover, classical SA strategies also do not leverage low rank structures with respect to parameters of parametric problems.

To tackle these issues, data-driven reduced-order models (ROMs) [19] can be utilized. ROM is a technique to build low rank approximations leveraging low rank structures in parametric problems. Recently, data-driven ROMs have been developed for RTE in [20, 21, 22, 23, 24, 25, 26, 27, 28, 29, 30, 31, 32, 33, 34]. In [35], under the SI framework, we employed a data-driven ROM for the ideal kinetic correction equation to design a ROM-enhanced SA strategy called ROMSAD to leverage the original kinetic description of the correction equation and low rank structures in parametric problems. The ideal kinetic correction equation varies as source iterations continue. To take this iteration dependence into account without consuming excessive memory, we built the ROM using the ideal corrections for the first few iterations. Without data for later iterations, the accuracy of the ROM may reduce as source iterations continue. Hence, in our ROMSAD method, we applied ROM-based corrections in the first few iterations to improve its efficiency and then switched to DSA to maintain robustness in later iterations. Using sufficiently accurate ROM, SI-ROMSAD is able to achieve significant acceleration over SI-DSA.

However, the ROMSAD preconditioner is only built for SI in [35], while Krylov solvers may be preferred in many applications for their faster convergence and better robustness. Additionally, the underlying ROM is constructed using high-fidelity ideal corrections for parameters across the entire training set, leading to potentially unnecessary computational costs due to the generation of all this high-fidelity data. In this paper, we extend our ROMSAD preconditioner from SI to the Krylov framework and apply a greedy algorithm [36, 34] to build the underlying ROM more efficiently.

1. To extend our method to the Krylov solver, following the extension of classical SA in [6], we first rewrite ROMSAD preconditioned SI as a Richardson iteration with a nonlinear left preconditioner solving a memory-efficient discrete formulation. Next, we identify the ideal kinetic correction equation in Krylov methods and reformulate it to efficiently obtain its solution without directly solving it. Due to the switching step in ROMSAD, the resulting preconditioner is nonlinear. Therefore, we choose the flexible general minimal residual method (FGMRES) [37] as the underlying Krylov solver.
2. When constructing the ROM, we use a greedy algorithm to iteratively enrich the underlying reduced order space by adding corrections for the most “representative” parameters. These “representative” parameters are identified by a residual-based error indicator. This greedy algorithm improves the offline efficiency by generating high-fidelity data only for the identified “representative” parameters rather than the entire training set.

Compared to our previous work [35], the main advancements are as follows. First, we reformulate the ideal kinetic correction equation for FGMRES to allow efficiently obtaining its solution without solving it. Second, we apply a greedy algorithm to improve the efficiency of the ROM construction.

Our numerical tests demonstrate that FGMRES with the ROMSAD preconditioner (FGMRES-ROMSAD) is more efficient than right preconditioned GMRES using the classical DSA preconditioner. Furthermore, when the underlying ROM is not highly accurate, FGMRES-ROMSAD is more robust than SI accelerated by ROMSAD.

Before detailing our method, we first contextualize it by briefly reviewing data-driven ROM-based accelerations of iterative linear solvers for RTE. Dynamic Mode Decomposition (DMD) is exploited as a low rank update strategy in SI [27] and eigenvalue solvers in [38, 39, 40]. A neural network surrogate for the transport sweep in SI is developed in [41]; however, this surrogate is only able to provide low-fidelity approximations. Random Singular Value Decomposition has been applied to build a low rank boundary-to-boundary map to enhance a Schwartz solver for RTE [42]. A ROM-based adaptive nested iterative solver is proposed for the Discontinuous Petrov Galerkin finite element method solving RTE [43]. Besides accelerations based on data-driven low rank approximations for RTE, Tailored Finite Point Method (TFPM) are utilized in [44, 45], while low rank matrix or tensor decomposition techniques are leveraged in the time marching [46, 47, 48, 49, 50, 51, 52] and iterative solvers of RTE [53].

Beyond the scope of RTE, ROM-based preconditioners have been developed for elliptic and parabolic problems in [54, 55, 56, 57, 58]. The ROM-based two-level preconditioner for elliptic equations in [55] shares similarities with the ROMSAD method, as both methods build single or multiple ROMs using data from multiple iterations. We will show that the projection step to construct the ROM-based preconditioner in these two methods has a major difference due to their distinct starting points. Our method is motivated by SA based on the ideal kinetic correction equation, while the method in [55] is inspired by two-grid preconditioners.

This paper is organized as follows. We briefly review the model equation and discretizations for it in Sec. 2, followed by basic ideas of classical SA in Sec. 3. Then, we outline how to extend ROMSAD method from SI to Krylov method and the greedy algorithm to build ROMs more efficiently in Sec. 4. The proposed method will be numerically tested in Sec. 5. At last, we draw our conclusions in Sec. 6.

## 2. Model equation and full order discretization

In this paper, we consider steady state linear RTE with one energy group, isotropic scattering, source and isotropic inflow boundary conditions:

$$\boldsymbol{\Omega} \cdot \nabla_{\mathbf{x}} \psi(\mathbf{x}, \boldsymbol{\Omega}) + \sigma_t(\mathbf{x}) \psi(\mathbf{x}, \boldsymbol{\Omega}) = \sigma_s(\mathbf{x}) \phi(\mathbf{x}) + G(\mathbf{x}), \quad \sigma_t(\mathbf{x}) = \sigma_s(\mathbf{x}) + \sigma_a(\mathbf{x}), \quad (1a)$$

$$\phi(\mathbf{x}) = \frac{1}{4\pi} \int_{\mathbb{S}^2} \psi(\mathbf{x}, \boldsymbol{\Omega}) d\boldsymbol{\Omega}, \quad \mathbf{x} \in \Gamma_{\mathbf{x}}, \quad (1b)$$

$$\psi(\mathbf{x}, \boldsymbol{\Omega}) = g(\mathbf{x}), \quad \mathbf{x} \in \partial\Gamma_{\mathbf{x}}, \quad \boldsymbol{\Omega} \cdot \mathbf{n}(\mathbf{x}) < 0. \quad (1c)$$

Here,  $\psi(\mathbf{x}, \boldsymbol{\Omega})$  is the angular flux (also known as radiation intensity or particle distribution) corresponding to angular direction on the unit sphere  $\boldsymbol{\Omega} = (\boldsymbol{\Omega}_x, \boldsymbol{\Omega}_y, \boldsymbol{\Omega}_z) \in \mathbb{S}^2$  and spatial location  $\mathbf{x} \in \Gamma_{\mathbf{x}}$ ,  $\phi(\mathbf{x}) = \frac{1}{4\pi} \int_{\mathbf{v} \in \mathbb{S}^2} \psi(\mathbf{x}, \boldsymbol{\Omega}) d\boldsymbol{\Omega}$  is the scalar flux (also known as the macroscopic density),  $G(\mathbf{x})$  is an isotropic source,  $\sigma_t(\mathbf{x}) = \sigma_s(\mathbf{x}) + \sigma_a(\mathbf{x}) \geq 0$  is the total cross section,  $\sigma_s(\mathbf{x}) \geq 0$  is the isotropic scattering cross section, and  $\sigma_a(\mathbf{x}) \geq 0$  is the absorption cross section. In the inflow boundary condition (1c),  $\mathbf{n}(\mathbf{x})$  is the outward normal direction of the computational domain  $\Gamma_{\mathbf{x}}$  at location  $\mathbf{x} \in \partial\Gamma_{\mathbf{x}}$ .

As the scattering effect goes to infinity, i.e.  $\sigma_s(\mathbf{x}) \rightarrow \infty$ , RTE (1) converges to its diffusion limit:  $\psi(\mathbf{x}, \boldsymbol{\Omega}) \rightarrow \phi(\mathbf{x})$  satisfying

$$-\nabla_x \cdot \left( \mathcal{D} \frac{1}{\sigma_s} \nabla \phi \right) = -\sigma_a \phi + G, \quad \text{where} \quad \mathcal{D} = \frac{1}{4\pi} \text{diag} \left( \int_{\mathbb{S}^2} \boldsymbol{\Omega}_x^2 d\boldsymbol{\Omega}, \int_{\mathbb{S}^2} \boldsymbol{\Omega}_y^2 d\boldsymbol{\Omega}, \int_{\mathbb{S}^2} \boldsymbol{\Omega}_z^2 d\boldsymbol{\Omega} \right). \quad (2)$$

When discretizing RTE (1), this diffusion limit need to be preserved on the discrete level. In other words, an asymptotic preserving method [59] should be applied to capture this diffusion limit without using a small mesh size  $h$  to resolve the mean free path of particles:  $\sigma_t h \ll 1$ . In this paper, we employ the discrete ordinates ( $S_N$ ) angular discretization and upwind discontinuous Galerkin (DG) spatial discretization, which is proved to be asymptotic preserving [5, 60].

### 2.1. Discrete ordinates ( $S_N$ ) angular discretization

The basic idea of the discrete ordinates ( $S_N$ ) method [3] is to sample the angular flux at a set of quadrature points  $\{\boldsymbol{\Omega}_j\}_{j=1}^{N_\Omega}$  with quadrature weights  $\{\omega_j\}_{j=1}^{N_\Omega}$  in the angular space. The scalar flux is approximated by the underlying quadrature rule. Here, we use a normalized quadrature rule  $\{(\boldsymbol{\Omega}_j, \omega_j)\}_{j=1}^{N_\Omega}$  satisfying

$$\sum_{j=1}^{N_\Omega} \omega_j = 1 \quad \text{and} \quad \frac{1}{4\pi} \int_{\mathbb{S}^2} g(\boldsymbol{\Omega}) d\boldsymbol{\Omega} \approx \sum_{j=1}^{N_\Omega} \omega_j g(\boldsymbol{\Omega}_j).$$

Then, the angular discretized version of (1) is given by:

$$(\boldsymbol{\Omega}_j \cdot \nabla_x + \sigma_t(\mathbf{x}))\psi(\mathbf{x}, \boldsymbol{\Omega}_j) = \sigma_s(\mathbf{x})\phi(\mathbf{x}) + G(\mathbf{x}, \boldsymbol{\Omega}_j), \quad \phi(\mathbf{x}) = \sum_{j=1}^{N_\Omega} \omega_j \psi(\mathbf{x}, \boldsymbol{\Omega}_j), \quad (3a)$$

$$\psi(\mathbf{x}, \boldsymbol{\Omega}_j) = g(\mathbf{x}), \quad \mathbf{x} \in \partial\Gamma_{\mathbf{x}}, \quad \boldsymbol{\Omega}_j \cdot \mathbf{n}(\mathbf{x}) < 0. \quad (3b)$$

In this paper, we use Chebyshev-Legendre (CL) quadrature rule. The CL quadrature rule  $\text{CL}(N_\theta, N_{\Omega_z})$  is the tensor product of the normalized  $N_\theta$ -points Chebyshev quadrature rule for the unit circle

$$\left\{ (\theta_j, \omega_{\theta,j}) : \theta_j = \frac{2j\pi}{N_\theta} - \frac{\pi}{N_\theta} \text{ and } \omega_j^\theta = \frac{1}{N_\theta}, j = 1, \dots, N_\theta \right\} \quad (4)$$

and the normalized  $N_{\Omega_z}$ -points Gauss-Legendre quadrature rule  $\{(\boldsymbol{\Omega}_{z,j}, \omega_{z,j})\}_{j=1}^{N_{\Omega_z}}$  for the  $z$ -component of angular direction  $\boldsymbol{\Omega}_z \in [-1, 1]$  satisfying  $\sum_{j=1}^{N_{\Omega_z}} \omega_{z,j} = 1$ . The quadrature points and the associated quadrature weights of the  $\text{CL}(N_\theta, N_{\Omega_z})$  quadrature rule are defined as

$$\boldsymbol{\Omega}_j = \left( \cos(\theta_{j_1}) \sqrt{1 - \boldsymbol{\Omega}_{z,j_2}^2}, \sin(\theta_{j_1}) \sqrt{1 - \boldsymbol{\Omega}_{z,j_2}^2}, \boldsymbol{\Omega}_{z,j_2} \right) \quad \text{and} \quad \omega_j = \omega_{\theta,j_1} \omega_{\Omega_z,j_2}, \quad (5)$$

where  $1 \leq j_1 \leq N_\theta$ ,  $1 \leq j_2 \leq N_{\Omega_z}$  and  $1 \leq j = (j_2 - 1)N_\theta + j_1 \leq N_{\Omega_z} N_\theta$ .

### 2.2. Upwind discontinuous Galerkin spatial discretization

For simplicity, we consider a 2D rectangular computational domain  $\Gamma_{\mathbf{x}} = [x_l, x_r] \times [y_l, y_r]$  and partition it with rectangular meshes  $\mathcal{T}_h = \{\mathcal{T}_i, \forall \mathcal{T}_i \text{ being rectangle}\}_{i=1}^{N_{\mathbf{x}}}$ . Denote the set of cell edges as  $\partial\mathcal{T}_h$  and the set of edges on the inflow boundary for  $\boldsymbol{\Omega}_j$  as

$$\partial\mathcal{T}_{h,j}^{(\text{ibc})} = \{\mathcal{E} : \mathcal{E} \in \partial\mathcal{T}_h, \mathcal{E} \subset \partial\Omega_{\mathbf{x}}, \boldsymbol{\Omega}_j \cdot \mathbf{n}(\mathbf{x}) < 0, \forall \mathbf{x} \in \mathcal{E}\},$$

where  $\mathbf{n}(\mathbf{x})$  is the outward normal direction of  $\Gamma_{\mathbf{x}}$  at  $\mathbf{x}$ .

To discretize the discrete ordinate equation (3) in space, we use a  $Q^K$  upwind discontinuous Galerkin (DG) method which seeks solution in the finite element space

$$U_h^K(\mathcal{T}_h) := \{u(\mathbf{x}) : u(\mathbf{x})|_{\mathcal{T}_i} \in Q^K(\mathcal{T}_i), 1 \leq i \leq N_{\mathbf{x}}\}. \quad (6)$$

Here,  $Q^K(\mathcal{T}_i)$  is the space of bi-variate polynomials on the element  $\mathcal{T}_i$  whose degree in each direction is at most

$K$ . Specifically, we seek  $\psi_h(\mathbf{x}, \boldsymbol{\Omega}_j) \in U_h^K(\mathcal{T}_h)$ ,  $j = 1, \dots, N_\Omega$  satisfying  $\forall \eta_h(\mathbf{x}) \in U_h^K(\mathcal{T}_h)$ ,

$$\begin{aligned} & - \sum_{i=1}^{N_x} \int_{\mathcal{T}_i} (\boldsymbol{\Omega}_j \cdot \nabla \eta_h(\mathbf{x})) \psi_h(\mathbf{x}, \boldsymbol{\Omega}_j) d\mathbf{x} + \sum_{\mathcal{E} \in \partial \mathcal{T}_h \setminus \partial \mathcal{T}_{h,j}^{(\text{ibc})}} \int_{\mathcal{E}} \widehat{\mathbf{H}}(\boldsymbol{\Omega}_j, \psi_h, \mathbf{n}(\mathbf{x})) \eta_h(\mathbf{x}) d\mathbf{x} + \sum_{i=1}^{N_x} \int_{\mathcal{T}_i} \sigma_t(\mathbf{x}) \psi_h(\mathbf{x}, \boldsymbol{\Omega}_j) \eta_h(\mathbf{x}) d\mathbf{x} \\ & = \sum_{i=1}^{N_x} \int_{\mathcal{T}_i} \sigma_s(\mathbf{x}) \phi_h(\mathbf{x}) \eta_h(\mathbf{x}) d\mathbf{x} + \sum_{i=1}^{N_x} \int_{\mathcal{T}_i} G(\mathbf{x}, \boldsymbol{\Omega}_j) \eta_h(\mathbf{x}) d\mathbf{x} - \sum_{\mathcal{E} \in \partial \mathcal{T}_{h,j}^{(\text{ibc})}} \int_{\mathcal{E}} g(\mathbf{x}, \boldsymbol{\Omega}_j) \phi_h(\mathbf{x}) \boldsymbol{\Omega}_j \cdot \mathbf{n}(\mathbf{x}) d\mathbf{x}. \end{aligned} \quad (7)$$

Here,  $\phi_h(\mathbf{x}) = \sum_{j=1}^{N_\Omega} \omega_j \psi_h(\mathbf{x}, \boldsymbol{\Omega}_j)$ . The upwind numerical flux  $\widehat{\mathbf{H}}(\boldsymbol{\Omega}_j, \psi_h, \mathbf{n}(\mathbf{x}))$  along the edge  $\mathcal{E}$  shared by an element  $\mathcal{T}^-$  and its neighbor  $\mathcal{T}^+$  is defined as

$$\widehat{\mathbf{H}}(\boldsymbol{\Omega}_j, \psi_h, \mathbf{n}(\mathbf{x})) \Big|_{\mathcal{E}} = \frac{\boldsymbol{\Omega}_j \cdot \mathbf{n}(\mathbf{x})}{2} (\psi_h^+(\mathbf{x}, \boldsymbol{\Omega}_j) + \psi_h^-(\mathbf{x}, \boldsymbol{\Omega}_j)) + \frac{|\boldsymbol{\Omega}_j \cdot \mathbf{n}(\mathbf{x})|}{2} (\psi_h^-(\mathbf{x}, \boldsymbol{\Omega}_j) - \psi_h^+(\mathbf{x}, \boldsymbol{\Omega}_j)), \quad (8)$$

where  $\psi_h^\pm(\mathbf{x}, \boldsymbol{\Omega}_j)$  is the restriction of  $\psi_h(\mathbf{x}, \boldsymbol{\Omega}_j)$  onto  $\mathcal{T}^\pm$ , and  $\mathbf{n}(\mathbf{x})$  is the unit outward normal direction with respect to the element  $\mathcal{T}^-$ . When the polynomial order  $K \geq 1$ , the above discrete ordinate DG method is asymptotic preserving [5, 60].

### 2.3. Matrix-vector formulation

Assume  $\{\eta_i(\mathbf{x})\}_{i=1}^{N_{\text{DOF}}}$  be an orthonormal basis for  $U_h^K(\mathcal{T}_h)$ . The degrees of freedom  $\boldsymbol{\psi}_j$  for  $\psi_h(\mathbf{x}, \boldsymbol{\Omega}_j)$  satisfies

$$\boldsymbol{\psi}_h(\mathbf{x}, \boldsymbol{\Omega}_j) = \boldsymbol{\psi}_j^T (\eta_1(\mathbf{x}), \dots, \eta_{N_{\text{DOF}}}(\mathbf{x}))^T = \sum_{k=1}^{N_{\text{DOF}}} \boldsymbol{\psi}_{j,k} \eta_k(\mathbf{x}). \quad (9)$$

The matrix-vector form of the fully discrete scheme is:

$$(\mathbf{D}_j + \boldsymbol{\Sigma}_t) \boldsymbol{\psi}_j = \boldsymbol{\Sigma}_s \mathbf{Q} \boldsymbol{\psi} + \mathbf{G} + \mathbf{g}_j^{(\text{bc})} = \boldsymbol{\Sigma}_s \boldsymbol{\phi} + \mathbf{G} + \mathbf{g}_j^{(\text{bc})} = \boldsymbol{\Sigma}_s \boldsymbol{\phi} + \widetilde{\mathbf{G}}_j, \quad (10a)$$

$$\boldsymbol{\psi} = (\boldsymbol{\psi}_1, \dots, \boldsymbol{\psi}_{N_\Omega})^T, \quad \boldsymbol{\phi} = \mathbf{Q} \boldsymbol{\psi} = \sum_{j=1}^{N_\Omega} \omega_j \boldsymbol{\psi}_j, \quad j = 1, \dots, N_\Omega. \quad (10b)$$

Here,  $\mathbf{Q} = \sum_{j=1}^{N_\Omega} \omega_j \boldsymbol{\psi}_j \in \mathbb{R}^{N_\Omega N_{\text{DOF}} \times N_{\text{DOF}}}$  is the discrete integration operator. The discrete advection operator  $\mathbf{D}_j \in \mathbb{R}^{N_{\text{DOF}} \times N_{\text{DOF}}}$ , the discrete scattering and total cross sections  $\boldsymbol{\Sigma}_s, \boldsymbol{\Sigma}_t \in \mathbb{R}^{N_{\text{DOF}} \times N_{\text{DOF}}}$ , the discrete source and boundary flux  $\mathbf{G}, \mathbf{g}_j^{(\text{bc})} \in \mathbb{R}^{N_{\text{DOF}}}$  are defined as:

$$(\mathbf{D}_j)_{kl} = - \sum_{i=1}^{N_x} \int_{\mathcal{T}_i} (\boldsymbol{\Omega}_j \cdot \nabla \eta_k(\mathbf{x})) \eta_l(\mathbf{x}) d\mathbf{x} + \sum_{\mathcal{E} \in \partial \mathcal{T}_h \setminus \partial \mathcal{T}_{h,j}^{(\text{ibc})}} \int_{\mathcal{E}} \widehat{\mathbf{H}}(\boldsymbol{\Omega}_j, \eta_l, \mathbf{n}(\mathbf{x})) \eta_k(\mathbf{x}) d\mathbf{x}, \quad (11a)$$

$$(\boldsymbol{\Sigma}_t)_{kl} = \sum_{i=1}^{N_x} \int_{\mathcal{T}_i} \sigma_t(\mathbf{x}) \eta_k(\mathbf{x}) \eta_l(\mathbf{x}) d\mathbf{x}, \quad (\boldsymbol{\Sigma}_s)_{kl} = \sum_{i=1}^{N_x} \int_{\mathcal{T}_i} \sigma_s(\mathbf{x}) \eta_k(\mathbf{x}) \eta_l(\mathbf{x}) d\mathbf{x}, \quad (11b)$$

$$(\mathbf{G})_k = \sum_{i=1}^{N_x} \int_{\mathcal{T}_i} G(\mathbf{x}) \phi_k(\mathbf{x}) d\mathbf{x}, \quad (\mathbf{g}_j^{(\text{bc})})_k = - \sum_{\mathcal{E} \in \partial \mathcal{T}_{h,j}^{(\text{ibc})}} \int_{\mathcal{E}} g(\mathbf{x}) \phi_k(\mathbf{x}) \boldsymbol{\Omega}_j \cdot \mathbf{n}(\mathbf{x}) d\mathbf{x}, \quad (11c)$$

$$\widetilde{\mathbf{G}}_j = \mathbf{G} + \mathbf{g}_j^{(\text{bc})}. \quad (11d)$$

Equation (10) can be further rewritten as a fully coupled system:

$$\mathbf{A}\boldsymbol{\psi} = \begin{pmatrix} \mathbf{D}_1 + \boldsymbol{\Sigma}_t - \omega_1 \boldsymbol{\Sigma}_s & -\omega_2 \boldsymbol{\Sigma}_s & \dots & -\omega_{N_\Omega} \boldsymbol{\Sigma}_s \\ -\omega_1 \boldsymbol{\Sigma}_s & \mathbf{D}_2 + \boldsymbol{\Sigma}_t - \omega_2 \boldsymbol{\Sigma}_s & \dots & -\omega_{N_\Omega} \boldsymbol{\Sigma}_s \\ \vdots & \vdots & \vdots & \vdots \\ -\omega_1 \boldsymbol{\Sigma}_s & -\omega_2 \boldsymbol{\Sigma}_s & \dots & \mathbf{D}_{N_\Omega} + \boldsymbol{\Sigma}_t - \omega_{N_\Omega} \boldsymbol{\Sigma}_s \end{pmatrix} \begin{pmatrix} \psi_1 \\ \psi_2 \\ \vdots \\ \psi_{N_\Omega} \end{pmatrix} = \begin{pmatrix} \tilde{\mathbf{G}}_1 \\ \tilde{\mathbf{G}}_2 \\ \vdots \\ \tilde{\mathbf{G}}_{N_\Omega} \end{pmatrix} = \mathbf{b}. \quad (12)$$

### 3. Krylov Solver and Source Iteration with Classical Synthetic Acceleration

In this section, we first briefly review the basic idea of Synthetic Acceleration (SA) under the Source Iteration (SI) framework [5, 7]. Then, following [6], we review how to extend SA to Krylov methods for faster convergence and enhanced robustness.

#### 3.1. Source Iteration and Synthetic Acceleration

Each iteration of SI-SA comprises a SI step and a SA step. In the  $l$ -th iteration, to avoid directly solving the fully coupled system (12), **the SI step** updates the angular flux  $\boldsymbol{\psi}$  by freezing the scalar flux  $\phi$ :

$$(\mathbf{D}_j + \boldsymbol{\Sigma}_t)\boldsymbol{\psi}_j^{(l)} = \boldsymbol{\Sigma}_s \phi^{(l-1)} + \tilde{\mathbf{G}}_j, \quad \phi^{(l,*)} = \sum_{j=1}^{N_\Omega} \omega_j \boldsymbol{\psi}_j^{(l)}, \quad \phi^{(0)} \text{ is given by an initial guess.} \quad (13)$$

With proper choices of basis functions in the upwind DG spatial discretization, the linear system  $\mathbf{D}_j + \boldsymbol{\Sigma}_s$  is block lower triangular if all elements are reordered along the upwind direction for  $\boldsymbol{\Omega}_j$ . After this reordering, equation (13) for each  $\boldsymbol{\Omega}_j$  can be solved with one block Gauss-Seidel iteration that sweeps along the upwind direction, namely transport sweep [12]. In practice, transport sweep is implemented in a matrix-free manner. Utilizing Fourier analysis, SI is proved to converge, but the convergence speed may be arbitrarily slow for scattering dominant problems [12].

**The SA step** accelerates the convergence of SI by introducing a correction to the scalar flux after each source iteration  $\phi^{(l)} = \phi^{(l,*)} + \delta\phi^{(l)}$ . The ideal correction  $\delta\phi^{(l)}$  is the difference between the true solution and the current solution  $\delta\phi^{(l)} = \phi - \phi^{(l,*)}$ . It satisfies an ideal discrete kinetic correction equation:

$$(\mathbf{D}_j + \boldsymbol{\Sigma}_t)\delta\boldsymbol{\psi}_j^{(l)} = \boldsymbol{\Sigma}_s \delta\phi^{(l)} + \boldsymbol{\Sigma}_s (\phi^{(l,*)} - \phi^{(l-1)}), \quad \delta\phi^{(l)} = \sum_{j=1}^{N_\Omega} \omega_j \delta\boldsymbol{\psi}_j^{(l)}. \quad (14)$$

This ideal correction equation can be rewritten as

$$\mathbf{A}\delta\boldsymbol{\psi}^{(l)} = \delta\mathbf{b}^{(l)} = \underbrace{\left( (\boldsymbol{\Sigma}_s(\phi^{(l,*)} - \phi^{(l-1)}))^T, \dots, (\boldsymbol{\Sigma}_s(\phi^{(l,*)} - \phi^{(l-1)}))^T \right)^T}_{\text{Repeat } N_\Omega \text{ times}}. \quad (15)$$

Using this ideal correction, SI converges in the next iteration. However, solving the ideal kinetic correction equation (14) is equally expensive as solving the original linear system (12).

In practice, instead of solving the ideal kinetic correction equation (14), we solve a computationally cheap low order approximation to it:

$$\mathbf{C}\delta\phi^{(l)} = \boldsymbol{\Sigma}_s(\phi^{(l,*)} - \phi^{(l-1)}), \quad (16)$$

and then correct the scalar flux as

$$\phi^{(l)} = \phi^{(l,*)} + \delta\phi^{(l)} = \phi^{(l,*)} + \mathbf{C}^{-1}\boldsymbol{\Sigma}_s(\phi^{(l,*)} - \phi^{(l-1)}). \quad (17)$$

The key of SA is to find a good low order approximation (16). Diffusion Synthetic Acceleration (DSA) [8, 9, 10, 11, 12] exploits the diffusion limit of the ideal correction equation and a discretization partially/fully consistent

with the upwind DG discretization (see Appendix A for details). Quasi-Diffusion methods [13, 14, 15] use the variable Eddington factor, while S2SA [16] utilizes the  $S_2$  angular discretization.

**Memory-efficient SI-SA:** Equation (13) gives

$$\boldsymbol{\psi}_j^{(l)} = (\mathbf{D}_j + \boldsymbol{\Sigma}_t)^{-1} \boldsymbol{\Sigma}_s \boldsymbol{\phi}^{(l-1)} + (\mathbf{D}_j + \boldsymbol{\Sigma}_t)^{-1} \tilde{\mathbf{G}}_j. \quad (18)$$

Numerically integrating equation (13) in the angular space, we obtain

$$\boldsymbol{\phi}^{(l,*)} = \mathbf{T} \boldsymbol{\Sigma}_s \boldsymbol{\phi}^{(l-1)} + \tilde{\mathbf{b}}, \quad \mathbf{T} = \sum_{j=1}^{N_\Omega} \omega_j (\mathbf{D}_j + \boldsymbol{\Sigma}_t)^{-1}, \quad \tilde{\mathbf{b}} = \sum_{j=1}^{N_\Omega} \omega_j (\mathbf{D}_j + \boldsymbol{\Sigma}_t)^{-1} \tilde{\mathbf{G}}_j. \quad (19)$$

Here, the operation of the operator  $\mathbf{T} = \sum_{j=1}^{N_\Omega} \omega_j (\mathbf{D}_j + \boldsymbol{\Sigma}_t)^{-1}$  is implemented based on numerical integration and matrix-free transport sweeps. Utilizing equation (19), SI-SA can be rewritten into a memory-efficient formulation only involving the scalar flux:

1. SI update:  $\boldsymbol{\phi}^{(l,*)} = \mathbf{T} \boldsymbol{\Sigma}_s \boldsymbol{\phi}^{(l-1)} + \tilde{\mathbf{b}}$ ;
2. SA correction:  $\boldsymbol{\phi}^{(l)} = \boldsymbol{\phi}^{(l,*)} + \mathbf{C}^{-1} \boldsymbol{\Sigma}_s (\boldsymbol{\phi}^{(l,*)} - \boldsymbol{\phi}^{(l-1)})$ .

With this formulation, there is no need to explicitly save the angular flux  $\boldsymbol{\psi}_j$ , however, the computational cost is almost the same as the original SI-SA in (13) due to the numerical integration and transport sweeps in the discrete operator  $\mathbf{T} = \sum_{j=1}^{N_\Omega} \omega_j (\mathbf{D}_j + \boldsymbol{\Sigma}_t)^{-1}$ .

### 3.2. GMRES with SA based preconditioner

**SI-SA as a Richardson iteration with left preconditioner:** Following [6], a preconditioner for discrete RTE can be constructed based on SA. Similar to the derivation of equation (19), we can derive the following equation from (10) :

$$\tilde{\mathbf{A}} \boldsymbol{\phi} = (\mathbf{I} - \mathbf{T} \boldsymbol{\Sigma}_s) \boldsymbol{\phi} = (\mathbf{I} - (\sum_{j=1}^{N_\Omega} \omega_j (\mathbf{D}_j + \boldsymbol{\Sigma}_t)^{-1}) \boldsymbol{\Sigma}_s) \boldsymbol{\phi} = \tilde{\mathbf{b}} \quad \text{and} \quad \tilde{\mathbf{b}} = \sum_{j=1}^{N_\Omega} \omega_j (\mathbf{D}_j + \boldsymbol{\Sigma}_t)^{-1} \tilde{\mathbf{G}}_j. \quad (20)$$

Vanilla SI without SA correction can be written as a Richardson iteration for (20):

$$\begin{aligned} \boldsymbol{\phi}^{(l)} &= \boldsymbol{\phi}^{(l,*)} = \mathbf{T} \boldsymbol{\Sigma}_s \boldsymbol{\phi}^{(l-1)} + \tilde{\mathbf{b}} \\ &= \boldsymbol{\phi}^{(l-1)} + (\tilde{\mathbf{b}} - (\mathbf{I} - \mathbf{T} \boldsymbol{\Sigma}_s) \boldsymbol{\phi}^{(l-1)}) \\ &= \boldsymbol{\phi}^{(l-1)} + \mathbf{r}^{(l-1)}. \end{aligned} \quad (21)$$

Equation (21) implies that the residual of the  $(l-1)$ -th iteration of the memory-efficient SI,  $\mathbf{r}^{(l-1)}$ , satisfies

$$\mathbf{r}^{(l-1)} = \boldsymbol{\phi}^{(l,*)} - \boldsymbol{\phi}^{(l-1)}. \quad (22)$$

Utilizing equation (17), (19) and (22), we rewrite SI-SA as

$$\begin{aligned} \boldsymbol{\phi}^{(l)} &= \boldsymbol{\phi}^{(l,*)} + \mathbf{C}^{-1} \boldsymbol{\Sigma}_s (\boldsymbol{\phi}^{(l,*)} - \boldsymbol{\phi}^{(l-1)}) \\ &= \boldsymbol{\phi}^{(l,*)} + \mathbf{C}^{-1} \boldsymbol{\Sigma}_s \mathbf{r}^{(l-1)} \\ &= \boldsymbol{\phi}^{(l-1)} + \mathbf{r}^{(l-1)} + \mathbf{C}^{-1} \boldsymbol{\Sigma}_s \mathbf{r}^{(l-1)} \\ &= \boldsymbol{\phi}^{(l-1)} + (\mathbf{I} + \mathbf{C}^{-1} \boldsymbol{\Sigma}_s) \mathbf{r}^{(l-1)}. \end{aligned} \quad (23)$$

Here,  $(\mathbf{I} + \mathbf{C}^{-1} \boldsymbol{\Sigma}_s) \mathbf{r}^{(l-1)} = (\mathbf{I} + \mathbf{C}^{-1} \boldsymbol{\Sigma}_s) (\tilde{\mathbf{b}} - (\mathbf{I} - \mathbf{T} \boldsymbol{\Sigma}_s) \boldsymbol{\phi}^{(l-1)})$  is the residual of the left preconditioned system

$$(\mathbf{I} + \mathbf{C}^{-1} \boldsymbol{\Sigma}_s) (\mathbf{I} - \mathbf{T} \boldsymbol{\Sigma}_s) \boldsymbol{\phi} = (\mathbf{I} + \mathbf{C}^{-1} \boldsymbol{\Sigma}_s) \tilde{\mathbf{b}}. \quad (24)$$

Comparing equation (21) and equation (23), we can see that introducing the SA step is equivalent to applying the left preconditioner  $\mathbf{I} + \mathbf{C}^{-1}\boldsymbol{\Sigma}_s$ .

**SA Preconditioned GMRES:** As discussed in [17, 6], SI-DSA may lose its efficiency and robustness for challenging problems with discontinuous materials. To accelerate the convergence and improve the robustness, SA preconditioners are extended to Krylov methods solving  $(\mathbf{I} - \mathbf{T}\boldsymbol{\Sigma}_s)\boldsymbol{\phi} = \mathbf{b}$ . Inspired by viewing SI-SA as a left preconditioned Richardson iteration, the left or right preconditioner for Krylov methods can be chosen as  $\mathbf{I} + \mathbf{C}^{-1}\boldsymbol{\Sigma}_s$ , where  $\mathbf{C}$  is the low order approximation to the ideal correction equation in the underlying SA.

### 3.3. Limitations of DSA

Classical DSA approximates the ideal kinetic correction equation (14) with its diffusion limit. However, it may become less effective, when the problem is far from its diffusion limit [18]. Moreover, the low rank structures of the solution manifold for the parametric problem is not leveraged.

## 4. Reduced order model enhanced preconditioner for Krylov method

To address the limitations of the classical DSA preconditioner, we exploit a ROM for the ideal correction equation to design a new SA preconditioner. This ROM is based on the original kinetic description of the ideal correction equation and leverages low rank structures in parametric problems. It is constructed following the offline-online decomposition approach. In the offline stage, we build the ROM by extracting low rank structures from data, specifically solutions to the ideal correction equation for parameters in a training set. In the online stage, to obtain high-fidelity solutions for a new parameter outside the training set, we apply a Krylov solver accelerated by the constructed ROM-enhanced preconditioner. Specifically, following our previous work to accelerate SI [35], we will use a hybrid SA preconditioner that utilizes ROM-based corrections in the first few iterations to improve efficiency and then switches to DSA for better robustness. Due to this switching, the resulting preconditioner is nonlinear. Hence, we choose flexible general minimal residual method (FGMRES) [61], allowing the use of nonlinear preconditioners, as our underlying Krylov solver.

In this section, we review the algorithm details of FGMRES in Sec. 4.1, outline our ROM-enhanced preconditioner in Sec. 4.2, and discuss how to construct the underlying ROM in Sec. 4.3.

### 4.1. Flexible GMRES

Following [37], we outline FGMRES in Alg. 1 which allows using a nonlinear preconditioner  $\mathbf{M}_j^{-1}$ . Here, the subscript  $j$  indicates the iteration dependence of the nonlinear preconditioner. The subtle but crucial difference between FGMRES and right preconditioned GMRES is that the preconditioned vectors  $\mathbf{z}^{(j)}$  are saved and utilized to update the solution. If the preconditioner is linear, i.e.  $\mathbf{M}_j^{-1} = \mathbf{M}^{-1}$  for any  $j$ , FGMRES is mathematically equivalent to right preconditioned GMRES.



---

**Algorithm 1** Flexible GMRES method to solve  $\tilde{\mathbf{A}}\phi = \tilde{\mathbf{b}}$  with a nonlinear preconditioner  $\mathbf{M}_j^{-1}$  [37].

---

- 1: Given an initial guess  $\phi^{(0)}$ , a nonlinear preconditioner  $\mathbf{M}_j^{-1}$ , and the maximum number of iterations allowed  $m$ .
  - 2: **Initialization:**
  - 3: **if**  $\|\phi^{(0)}\|_2 == 0$  **then**
  - 4:    $\mathbf{r}^{(0)} = \tilde{\mathbf{b}}$ ,
  - 5: **else**
  - 6:    $\mathbf{r}^{(0)} = \tilde{\mathbf{b}} - \tilde{\mathbf{A}}\phi^{(0)}$ .
  - 7: **end if**
  - 8: Define  $\beta = \|\mathbf{r}^{(0)}\|_2$  and  $\mathbf{v}^{(1)} = \mathbf{r}^{(0)}/\beta$ . Allocate the memory for the Hessenberg matrix  $\mathbf{H} \in \mathbb{R}^{(m+1) \times m}$ .
  - 9: **Anorlidi process:**
  - 10: **for**  $j = 1 : m$  **do**
  - 11:   **Apply the nonlinear preconditioner:**  $\mathbf{z}^{(j)} := \mathbf{M}_j^{-1}\mathbf{v}^{(j)}$ .
  - 12:   Compute  $\mathbf{w} := \tilde{\mathbf{A}}\mathbf{z}^{(j)}$ .
  - 13:   **for**  $i = 1 : j$  **do**
  - 14:      $\mathbf{H}_{ij} = \mathbf{w}^T \mathbf{v}^{(i)}$ , and update  $\mathbf{w} = \mathbf{w} - \mathbf{H}_{ij}\mathbf{v}^{(i)}$ .
  - 15:   **end for**
  - 16:   Compute  $\mathbf{H}_{j+1,j} = \|\mathbf{w}\|_2$ .
  - 17:   Update  $\mathbf{v}^{(j+1)} = \mathbf{w}/\mathbf{H}_{j+1,j}$ .
  - 18:   **if** Stopping criteria satisfied **then**
  - 19:     Stop iterations.
  - 20:   **end if**
  - 21: **end for**
  - 22: **Obtain the solution:**
  - 23: Define  $\tilde{\mathbf{Z}} = (\mathbf{z}^{(1)}, \mathbf{z}^{(2)}, \dots, \mathbf{z}^{(j)})$  and  $\tilde{\mathbf{H}} = (\mathbf{H}_1, \mathbf{H}_2, \dots, \mathbf{H}_j)$ . Solve the minimization problem  $\mathbf{y}^* = \arg \min_{\mathbf{y} \in \mathbb{R}^j} \|\beta \mathbf{e}_1 - \tilde{\mathbf{H}}\mathbf{y}\|_2$ , where  $\mathbf{e}_1 = (1, 0, \dots, 0)^T \in \mathbb{R}^j$ .
  - 24: Compute and return  $\phi := \phi^{(0)} + \tilde{\mathbf{Z}}\mathbf{y}^*$ .
- 

#### 4.2. ROM-enhanced SA preconditioner

To leverage the original kinetic description of the correction equation and low rank structures in parametric problems, we propose a SA strategy combining ROM-based SA and DSA, called ROMSAD, under the SI framework in [35]. Here, we briefly review its basic ideas and outline how to extend it to the Krylov framework.

We follow an offline-online decomposition framework. In the offline stage, we find low rank structures in parametric problems from data, and construct a reduced order space whose bases are column vectors of  $\mathbf{U}_r \in \mathbb{R}^{N_\Omega \times N_{\text{DOF}} \times r}$ . We denote rows corresponding to degrees of freedom for  $\psi_h(\cdot, \Omega_j)$  in  $\mathbf{U}_r = (\mathbf{U}_{r,1}^T, \dots, \mathbf{U}_{r,N_\Omega}^T)^T$  as  $\mathbf{U}_{r,j} \in \mathbb{R}^{N_{\text{DOF}} \times r}$ . In the online stage, we seek the correction by projecting the ideal kinetic correction equation (15) onto the reduced order space  $\mathbf{U}_r$ :

$$\mathbf{U}_r^T \mathbf{A} \mathbf{U}_r \mathbf{c}_r^{(l)} = \mathbf{U}_r^T \delta \mathbf{b}^{(l)} = \sum_{j=1}^{N_\Omega} \mathbf{U}_{r,j}^T \boldsymbol{\Sigma}_s (\phi^{(l,*)} - \phi^{(l-1)}) = \left( \sum_{j=1}^{N_\Omega} \mathbf{U}_{r,j} \right)^T \boldsymbol{\Sigma}_s \mathbf{r}^{(l-1)}, \quad \mathbf{c}_r^{(l)} \in \mathbb{R}^r, \quad (25a)$$

$$\delta \boldsymbol{\psi}^{(l)} \approx \mathbf{U}_r \mathbf{c}_r^{(l)}, \quad \delta \phi^{(l)} = \sum_{j=1}^{N_\Omega} \omega_j \boldsymbol{\psi}_j^{(l)} \approx \sum_{j=1}^{N_\Omega} \omega_j \mathbf{U}_{r,j} \mathbf{c}_r^{(l)} = \left( \sum_{j=1}^{N_\Omega} \omega_j \mathbf{U}_{r,j} \right) \mathbf{c}_r^{(l)}. \quad (25b)$$

Our ROMSAD method uses ROM-based corrections in (25) for the first few iterations and then switches to DSA. We need this switching, as the ROM is constructed only using the data for the first few iterations, i.e.  $\delta \boldsymbol{\psi}^{(l)}$ ,  $1 \leq l \leq \mathfrak{w}$ , to avoid excessive memory costs due to the high dimensionality of the angular flux.

To extend ROMSAD method to the Krylov framework, we need to derive the correction operator “ $\mathbf{C}^{-1}$ ”

in (17) for the ROM-based correction. Based on (25), we have

$$\delta\phi^{(l)} = \sum_{j=1}^{N_\Omega} \omega_j \delta\psi_j^{(l)} \approx \left( \sum_{j=1}^{N_\Omega} \omega_j \mathbf{U}_{r,j} \right) (\mathbf{U}_r^T \mathbf{A} \mathbf{U}_r)^{-1} \left( \sum_{j=1}^{N_\Omega} \mathbf{U}_{r,j} \right)^T \boldsymbol{\Sigma}_s \mathbf{r}^{(l-1)}. \quad (26)$$

Comparing (17) and (26), we conclude  $\mathbf{C}_{\text{ROM}}^{-1} = \left( \sum_{j=1}^{N_\Omega} \omega_j \mathbf{U}_{r,j} \right) (\mathbf{U}_r^T \mathbf{A} \mathbf{U}_r)^{-1} \left( \sum_{j=1}^{N_\Omega} \mathbf{U}_{r,j} \right)^T$ . Following Sec. 3.2, the SA preconditioner corresponding to this ROM correction is

$$\mathbf{M}_{\text{ROM}}^{-1} = \mathbf{I} + \mathbf{C}_{\text{ROM}}^{-1} \boldsymbol{\Sigma}_s = \mathbf{I} + \left( \sum_{j=1}^{N_\Omega} \omega_j \mathbf{U}_{r,j} \right) (\mathbf{U}_r^T \mathbf{A} \mathbf{U}_r)^{-1} \left( \sum_{j=1}^{N_\Omega} \mathbf{U}_{r,j} \right)^T \boldsymbol{\Sigma}_s. \quad (27)$$

Then, the nonlinear ROMSAD preconditioner for the  $j$ -th iteration of FGMRES can be defined as

$$\mathbf{M}_j^{-1} = \begin{cases} \mathbf{M}_{\text{ROM}}^{-1}, & 1 \leq j \leq \mathfrak{w}, \\ \mathbf{M}_{\text{DSA}}^{-1}, & \text{otherwise.} \end{cases} \quad (28)$$

Here, the window size,  $\mathfrak{w}$ , is defined as the number of iterations whose data are utilized in the ROM construction, and  $\mathbf{M}_{\text{DSA}}^{-1}$  is the DSA-preconditioner. We want to point out that a more complicated switching strategy is used in our previous work for SI [35]. Due to the better robustness of Krylov method, the switching strategy in (28) works well for all our numerical tests.

A key point in our method is that the ROM is directly built for the ideal kinetic correction equation (14) instead of the corresponding memory-efficient formulation,  $(\mathbf{I} - \mathbf{T} \boldsymbol{\Sigma}_s) \delta\phi^{(l)} = \delta\mathbf{b}$ , because the operator  $\mathbf{T} = \sum_{j=1}^{N_\Omega} \omega_j (\mathbf{D}_j + \boldsymbol{\Sigma}_t)^{-1}$  depends on the total cross section  $\sigma_t$  in a non-affine manner. Due to this non-affine dependence, whenever the total cross section  $\sigma_t$  is parametric, projection-based ROM for the memory-efficient formulation may lose its online efficiency [24]. Classical empirical interpolation method (EIM) [62] and discrete EIM [63] tackle the efficiency loss due to non-affine dependence by sub-sampling rows of reduced order matrices and vectors. However, if  $\mathbf{T}$  is implemented via a matrix-free transport sweep, computing the outputs of the sampled row requires computing all “previous rows along the upwind direction” first. Consequently, when the matrix-free transport sweep is applied, simply applying EIM and DEIM may not achieve the desired efficiency boost.

**Remark 4.1.** *Our ROM-based SA preconditioner is different from directly extending the ROM-based preconditioner for elliptic equations [55] to RTE, as the starting points for these two methods are different. Based on the SA framework, our ROM-based SA preconditioner is*

$$\mathbf{I} + \sum_{j=1}^{N_\Omega} (\omega_j \mathbf{U}_{r,j}) (\mathbf{U}_r^T \mathbf{A} \mathbf{U}_r)^{-1} \left( \sum_{j=1}^{N_\Omega} \mathbf{U}_{r,j} \right)^T \boldsymbol{\Sigma}_s.$$

[55] derives a ROM-based preconditioner by replacing the “coarse grid space” in two-grid methods with a reduced order space. Directly applying [55] to the memory-efficient formulation of RTE (20) results in the preconditioner  $\tilde{\mathbf{U}}_r \left( \tilde{\mathbf{U}}_r^T (\mathbf{I} - \mathbf{T} \boldsymbol{\Sigma}_t) \tilde{\mathbf{U}}_r \right)^{-1} \tilde{\mathbf{U}}_r^T$  where  $\tilde{\mathbf{U}}_r$  is the reduced order basis for a ROM of the memory-efficient formulation. Clearly, this direct extension of [55] may suffer from the efficiency loss due to the aforementioned non-affine issue.

#### 4.3. ROM construction

The only remaining question is how to build the ROM for the ideal kinetic correction equation. To answer this question, we first figure out the ideal kinetic correction equation for FGMRES and then rewrite it into an equivalent form to obtain its solution efficiently without solving it. Then, we build the ROM using a greedy algorithm [36] that iteratively identifies representative parameters from a training set based on a

residual-based error indicator. Using this strategy, we only need to generate the high-fidelity ideal angular flux corrections for these identified parameters, while our previous work [35], constructed the ROM by proper orthogonal decomposition (POD) using high-fidelity data for all parameters in a training set. Consequently, the underlying ROM may be constructed more efficiently compared to [35].

#### 4.3.1. Ideal correction under the Krylov framework and data generation

As discussed in the last paragraph of Sec. 4.2, we need to construct the ROM for the kinetic correction equation instead of its memory-efficient formulation to avoid the non-affine issues. Here, we identify the ideal kinetic correction equation for FGMRES as follows.

Recall that, under the SI framework, the residual for the  $(l-1)$ -th iteration,  $\mathbf{r}^{(l-1)}$ , satisfies  $\mathbf{r}^{(l-1)} = \phi^{(l,*)} - \phi^{(l-1)}$ . Substituting this relation into equation (13), the ideal angular flux correction for SI can be rewritten as:

$$(\mathbf{D}_j + \Sigma_t)\delta\psi_j^{(l)} = \Sigma_s\delta\phi^{(l)} + \Sigma_s\mathbf{r}^{(l-1)}, \quad \delta\phi^{(l)} = \sum_{j=1}^{N_\Omega} \omega_j\delta\psi_j^{(l)}, \quad 1 \leq j \leq N_\Omega. \quad (29)$$

In the preconditioning step of FGMRES, the residual in SI,  $\mathbf{r}^{(l-1)}$ , is replaced by the orthogonal basis of the Krylov space  $\mathbf{v}^{(l)}$ . Therefore, the ideal angular flux correction for FGMRES, namely  $\delta\psi_j^{(l)}$ , solves

$$(\mathbf{D}_j + \Sigma_t)\delta\psi_j^{(l)} = \Sigma_s\delta\phi^{(l)} + \Sigma_s\mathbf{v}^{(l)}, \quad \delta\phi^{(l)} = \sum_{j=1}^{N_\Omega} \omega_j\delta\psi_j^{(l)}, \quad j = 1, \dots, N_\Omega. \quad (30)$$

We will show that the ideal angular flux correction satisfying (30), namely  $\delta\psi^{(l)}$ , is also the solution to the following equation:

$$(\mathbf{D}_j + \Sigma_t)\delta\psi_j^{(l)} = \Sigma_s\delta\bar{\phi}^{(l)}, \quad j = 1, \dots, N_\Omega, \quad (31a)$$

$$\tilde{\mathbf{A}}\delta\bar{\phi}^{(l)} = \mathbf{v}^{(l)}, \quad \delta\phi^{(l)} = \sum_{j=1}^{N_\Omega} \omega_j\delta\phi_j^{(l)}. \quad (31b)$$

Equation (31a) results in

$$\delta\psi_j^{(l)} = (\mathbf{D}_j + \Sigma_t)^{-1}\Sigma_s\delta\bar{\phi}^{(l)}, \quad j = 1, \dots, N_\Omega, \quad (32)$$

$$\delta\phi^{(l)} = \sum_{j=1}^{N_\Omega} \omega_j\psi_j^{(l)} = \left(\sum_{j=1}^{N_\Omega} \omega_j(\mathbf{D}_j + \Sigma_t)^{-1}\right)\Sigma_s\delta\bar{\phi}^{(l)} = \mathbf{T}\Sigma_s\bar{\phi}^{(l)}. \quad (33)$$

Therefore, equation (31a) and (33) lead to

$$\begin{aligned} (\mathbf{D}_j + \Sigma_t)\delta\psi_j^{(l)} - \Sigma_s\delta\phi^{(l)} &= \Sigma_s\delta\bar{\phi}^{(l)} - \Sigma_s(\mathbf{T}\Sigma_s\delta\bar{\phi}^{(l)}) \\ &= \Sigma_s(\mathbf{I} - \mathbf{T}\Sigma_s)\delta\bar{\phi}^{(l)} = \Sigma_s\tilde{\mathbf{A}}\delta\bar{\phi}^{(l)} = \Sigma_s\mathbf{v}^{(l)}. \end{aligned} \quad (34)$$

Moving  $\Sigma_s\delta\phi^{(l)}$  to the right-hand side, we show that the solution to (31) is also the solution to the ideal kinetic correction equation (30).

Utilizing (31), snapshots for the ideal angular flux corrections can be efficiently constructed as long as we can efficiently compute the solution to  $\tilde{\mathbf{A}}\delta\bar{\phi}^{(l)} = \mathbf{v}^{(l)}$  without directly solving it or using matrix-vector multiplications determined by  $\tilde{\mathbf{A}}$ . Similar to [55], this can be achieved by utilizing the definition of FGMRES

method in Alg. 1. In the first iteration, we have

$$\begin{aligned}\tilde{\mathbf{A}}\delta\bar{\phi}^{(1)} &= (\mathbf{I} - \mathbf{T}\Sigma_t)\delta\bar{\phi}^{(1)} = \mathbf{v}^{(1)} = \mathbf{r}^{(0)}/\beta = \mathbf{r}^{(0)}/\|\mathbf{r}^{(0)}\|_2 = (\tilde{\mathbf{b}} - \tilde{\mathbf{A}}\phi^{(0)})/\|\mathbf{r}^{(0)}\|, \\ \delta\bar{\phi}^{(1)} &= \tilde{\mathbf{A}}^{-1}(\tilde{\mathbf{b}} - \tilde{\mathbf{A}}\phi^{(0)})/\|\mathbf{r}^{(0)}\|_2 = \tilde{\mathbf{A}}^{-1}(\tilde{\mathbf{A}}\phi - \tilde{\mathbf{A}}\phi^{(0)})/\|\mathbf{r}^{(0)}\|_2 = (\phi - \phi^{(0)})/\|\mathbf{r}^{(0)}\|_2,\end{aligned}\quad (35)$$

where  $\phi$  is the solution to  $\tilde{\mathbf{A}}\phi = (\mathbf{I} - \mathbf{T}\Sigma_t)\phi = \tilde{\mathbf{b}}$ , which can be well approximated by the converged solution of FGMRES. As a result, to compute  $\delta\bar{\phi}^{(1)}$ , we only need to save the converged solution  $\phi$  and the initial guess  $\phi^{(0)}$ . Similarly, based on line 12 to line 17 of Alg. 1, we can show that  $\delta\bar{\phi}^{(l)}$  for  $l \geq 2$  satisfying

$$\begin{aligned}\tilde{\mathbf{A}}\delta\bar{\phi}^{(l)} &= \mathbf{v}^{(l)} = (\tilde{\mathbf{A}}\mathbf{z}^{(l-1)} - \sum_{i=1}^{l-1} \mathbf{H}_{i,l-1}\mathbf{v}^{(i)})/\mathbf{H}_{l,l-1}, \quad l \geq 2, \\ \delta\bar{\phi}^{(l)} &= \tilde{\mathbf{A}}^{-1}(\tilde{\mathbf{A}}\mathbf{z}^{(l-1)} - \sum_{i=1}^{l-1} \mathbf{H}_{i,l-1}\mathbf{v}^{(i)})/\mathbf{H}_{l,l-1} = \frac{1}{\mathbf{H}_{l,l-1}} \left( \mathbf{z}^{(l-1)} - \sum_{i=1}^{l-1} \mathbf{H}_{i,l-1}\tilde{\mathbf{A}}^{-1}\mathbf{v}^{(i)} \right) \\ &= \frac{1}{\mathbf{H}_{l,l-1}} \left( \mathbf{z}^{(l-1)} - \sum_{i=1}^{l-1} \mathbf{H}_{i,l-1}\delta\bar{\phi}^{(i)} \right), \quad l \geq 2.\end{aligned}\quad (36)$$

Utilizing (35) and (36), we can iteratively compute  $\delta\bar{\phi}^{(l)}$  for the first  $\mathfrak{w}$  iterations, by saving the converged solution, elements in the matrix  $\mathbf{H}$ , vectors  $\mathbf{z}^{(l)}$  and  $\mathbf{v}^{(l)}$ .

In summary, under FGMRES framework, to generate the ideal angular flux corrections  $\delta\psi^{(l)}$  for the first few iterations  $1 \leq l \leq \mathfrak{w}$ , we first compute  $\delta\bar{\phi}^{(l)}$  iteratively using (35) and (36). Then, we construct the ideal angular flux corrections  $\delta\psi^{(l)}$  by applying  $\mathfrak{w}$  additional transport sweeps to solve (31a). Using this two-step strategy, we generate  $\delta\psi^{(l)}$  while avoiding directly solving (30) or using matrix-vector multiplications determined by  $\tilde{\mathbf{A}}$ .

#### 4.3.2. Greedy algorithm to build ROM

In the offline stage, we will use a greedy algorithm to build a ROM for the ideal kinetic correction equation for FGMRES (30). The author is aware that a systematic study of greedy algorithms to build ROMs for parametric RTE is ongoing [34]. The greedy algorithm iteratively enriches the reduced order space by sampling the most representative parameters from the training set. These representative parameters are identified by a residual-based error indicator. High-fidelity linear solves are only needed to generate data for these sampled parameters.

Before going to details of the greedy algorithm, we first introduce our notations and assumptions. Let the full order problem (12) for the parameter  $\mu$  be  $\mathbf{A}_\mu\psi_\mu = \mathbf{b}_\mu$ , and the equivalent memory-efficient formulation be  $\tilde{\mathbf{A}}_\mu\phi_\mu = \tilde{\mathbf{b}}_\mu$ . Here,  $\mu$  is the parameter of the parametric problem, such as the parametrization of material properties or boundary conditions. The subscript  $\mu$  denotes the  $\mu$ -dependence. Additionally, for simplicity, we assume the operator  $\mathbf{A}_\mu$  depends on the parameter  $\mu$  in an affine manner, i.e.  $\mathbf{A}_\mu = \sum_{s=1}^m a_s(\mu)\mathbf{A}_s$ , where  $\mathbf{A}_s$ 's are constant matrices independent of  $\mu$ . Then, given the reduced basis  $\mathbf{U}_r$ , the reduced order operator for any  $\mu$  can be fast constructed online as  $\mathbf{U}_r^T\mathbf{A}_\mu\mathbf{U}_r = \sum_{s=1}^m a_s(\mu)\mathbf{A}_{s,r}$ , where  $\mathbf{A}_{s,r} = \mathbf{U}_r^T\mathbf{A}_s\mathbf{U}_r$  are precomputed and saved offline. Note that, projecting the matrix  $\mathbf{A}_\mu$  does not require matrix-free transport sweep, so EIM [62] and DEIM [63] can be applied when  $\mathbf{A}_\mu$  has non-affine dependence on  $\mu$ .

We use FGMRES with DSA preconditioner, which is equivalent to right preconditioned GMRES, and zero initial guess to generate required high-fidelity data. The steps of the greedy algorithm are as follows.

**Input:** The training set of parameters  $\mathcal{P}_{\text{train}} = \{\mu_s\}_{s=1}^{N_{\text{train}}}$ , maximum number of greedy iterations  $N_{\text{g-iter}}$ , the window size  $\mathfrak{w}$  determining high-fidelity data for how many iterations will be used, the initial sample  $\mu_1$  and the tolerance for the residual  $\epsilon_{\text{rom}}$ ,

##### 1. Preparation and initialization.

Use (19) to compute the right-hand side of the memory-efficient formulation  $\tilde{\mathbf{b}}_\mu$  for all  $\mu \in \mathcal{P}_{N_{\text{train}}}$ . Since zero initial guesses are applied, the initial residuals for FGMRES are  $\mathbf{r}_\mu^{(0)} = \tilde{\mathbf{b}}_\mu = \|\mathbf{r}_\mu^{(0)}\|_2 \mathbf{v}^{(1)}$ . Compute and save  $\boldsymbol{\eta}_\mu^{(0)} = \boldsymbol{\Sigma}_s \mathbf{r}_\mu^{(0)}$ . Set  $k = 1$ , and the set of sampled parameters as  $\mathcal{P}_{\text{sampled}} = \{\mu_1\}$ .

## 2. Update reduced order basis.

- (a) **High fidelity solve for sampled parameters.** Use FGMRES to solve  $\tilde{\mathbf{A}}_{\mu_k} \phi_{\mu_k} = \tilde{\mathbf{b}}_{\mu_k}$ . Use (35) and (36) to compute the solution to  $\tilde{\mathbf{A}} \delta \bar{\phi}_{\mu_k}^{(l)} = \mathbf{v}_{\mu_k}^{(l)}$ ,  $\delta \bar{\phi}_{\mu_k}^{(l)}$ , for  $1 \leq l \leq \mathfrak{w}$ .
- (b) **Compute angular flux corrections.** Generate the angular flux correction  $\delta \psi_{\mu_k}^{(l)}$  for  $1 \leq l \leq \mathfrak{w}$  by solving (31a) with transport sweeps.
- (c) **Update reduced order basis and operators.** Apply the modified Gram-Schmidt procedure to update  $\mathbf{U}_r$  by adding columns orthogonal to its existing columns from the column space of the snapshot matrix  $\mathbf{S}_{\mu_k} = [\delta \psi_{\mu_k}^{(1)}, \dots, \delta \psi_{\mu_k}^{(\mathfrak{w})}]$ , and then update reduced order operators correspondingly. If  $k$  equal to  $N_{\text{g-iter}}$ , stop. Otherwise, go to step 3.

## 3. Greedy sampling.

- (a) **Generate reduced order solutions.** For all unsampled parameters,  $\mu \in \mathcal{P}_{\text{train}} \setminus \mathcal{P}_{\text{sampled}}$ , compute the reduced order angular flux of the correction equation for the first iteration of FGMRES:

$$\mathbf{U}_r^T \mathbf{A}_\mu \mathbf{U}_r \mathbf{c}_{r,\mu} = \left( \sum_{j=1}^{N_\Omega} \mathbf{U}_{r,j} \right)^T \boldsymbol{\Sigma}_s \mathbf{r}_\mu^{(0)} = \|\mathbf{r}_\mu^{(0)}\|_2 \left( \sum_{j=1}^{N_\Omega} \mathbf{U}_{r,j} \right)^T \boldsymbol{\Sigma}_s \mathbf{v}^{(1)} = \left( \sum_{j=1}^{N_\Omega} \mathbf{U}_{r,j}^T \right) \boldsymbol{\eta}_\mu^{(0)}, \quad \mathbf{c}_{r,\mu} \in \mathbb{R}^r \quad (37a)$$

$$\delta \psi_{\mu,\text{ROM}} \approx \mathbf{U}_r \mathbf{c}_r, \quad \delta \phi_{\mu,\text{ROM}} \approx \sum_{j=1}^{N_\Omega} \omega_j \mathbf{U}_{r,j} \mathbf{c}_r. \quad (37b)$$

- (b) **Greedy sampling based on residuals.** Compute the residual of the current reduced order solutions

$$\begin{aligned} \mathcal{R}_\mu &= \max_{1 \leq j \leq N_\Omega} \|(\mathbf{D}_j + \boldsymbol{\Sigma}_{t,\mu}) \delta \psi_{j,\text{ROM}} - \boldsymbol{\Sigma}_{s,\mu} \delta \phi_{\text{ROM}} - \boldsymbol{\Sigma}_{s,\mu} \mathbf{r}_\mu^{(0)}\|_2 \\ &= \max_{1 \leq j \leq N_\Omega} \|(\mathbf{D}_j + \boldsymbol{\Sigma}_{t,\mu}) \delta \psi_{j,\text{ROM}} - \boldsymbol{\Sigma}_{s,\mu} \delta \phi_{\text{ROM}} - \boldsymbol{\eta}_\mu^{(0)}\|_2. \end{aligned} \quad (38)$$

If  $\max_{\mu \in \mathcal{P}_{\text{train}} \setminus \mathcal{P}_{\text{sampled}}} \{\mathcal{R}_\mu\} < \epsilon_{\text{rom}}$ , stop the algorithm. Otherwise, sample  $\mu_{k+1}$  as

$$\mu_{k+1} = \arg \max_{\mu \in \mathcal{P}_{\text{train}} \setminus \mathcal{P}_{\text{sampled}}} \{\mathcal{R}_\mu\},$$

then update  $\mathcal{P}_{\text{sampled}} := \mathcal{P}_{\text{sampled}} \cup \{\mu_{k+1}\}$  and  $k := k + 1$ . Go back to step 2.

## 4. Output: the reduced order basis $\mathbf{U}_r$ and corresponding reduced order operators.

In our greedy algorithm, representative parameters are sampled based on the correction equation only for the first iteration of FGMRES, because given the initial guess and the right-hand side, they can be easily computed in the preparation step. Though we use zero initial guesses in this paper, the greedy method can be straightforwardly extended to other initial guesses.

Compared with the POD method used in our previous work [35], the greedy algorithm reduces the number of high-fidelity solves with the additional cost of greedy sampling. Our numerical tests demonstrate that, when the number of representative parameters is smaller than the size of the training set, this additional cost is marginal compared to generating the high-fidelity data for the entire training set.

## 5. Numerical results

We will utilize a series of numerical examples in the 2D X-Y geometry to test the performance of FGMRES with the ROMSAD preconditioner (FGMRES-ROMSAD). We will compare its performance to GMRES with right DSA preconditioner (GMRES-DSA), since FGMRES with a linear preconditioner is mathematically equivalent to right preconditioned GMRES. Throughout this section, we use a linear DG space ( $K = 1$ ) for the spatial discretization. For the DSA preconditioner, we will use the fully consistent version described in Appendix A, unless otherwise specified. We observe that, in comparison with the partially consistent version, the fully consistent one results in less number of iterations for convergence and computational time for our numerical examples. When solving the diffusion equation in DSA, we employ an algebraic multigrid (AMG) solver implemented based on the iFEM package [64].

The online performance of the proposed method is tested with a test set of parameters  $\mathcal{P}_{\text{test}}$  that lies outside the training set  $\mathcal{P}_{\text{train}}$ . We define the average number of transport sweeps for the test set as

$$\bar{n}_{\text{sweep}} = \frac{\sum_{\boldsymbol{\mu} \in \mathcal{P}_{\text{train}}} \text{number of transport sweeps for convergence for the parameter } \boldsymbol{\mu}}{\text{total number of parameters in } \mathcal{P}_{\text{test}}}.$$

In high dimensions, when many angular directions are used in the angular discretization, the computational cost of applying DSA or ROMSAD preconditioners is marginal compared to transport sweeps. Thus, the average computational time is approximately proportional to  $\bar{n}_{\text{sweep}}$ . To verify that iterative solvers converge to the correct solution, we compute the average  $l_\infty$  residual:

$$\bar{\mathcal{R}}_\infty = \frac{\sum_{\boldsymbol{\mu} \in \mathcal{P}_{\text{test}}} \|(\mathbf{I} - \mathbf{T}\boldsymbol{\Sigma}_s)\boldsymbol{\rho}_\mu - \tilde{\mathbf{b}}_\mu\|_\infty}{\text{total number of parameters in } \mathcal{P}_{\text{test}}},$$

where  $\boldsymbol{\rho}_\mu$  is the numerical solution obtained by the underlying iterative solver. We define the average relative computational time  $\bar{T}_{\text{rel}}$  with respect to GMRES-DSA.

**Remark 5.1.** *We want to point out that when a zero initial guess is used in FGMRES (see Alg. 1), the number of transport sweeps required for convergence is equal to one plus the number of iterations, as one transport sweep is needed to compute the right-hand side of the memory-efficient formulation,  $\tilde{\mathbf{b}}$ , based on (20). When other initial guesses are employed, an additional transport sweep will be needed to compute the initial residual.*

### 5.1. Lattice problem

We consider a parametric lattice problem with zero inflow boundary conditions in the computational domain  $\Gamma_{\mathbf{x}} = [0, 5]^2$ . The setup is presented in the left picture of Fig. 1, where the black regions are pure absorption regions with  $(\sigma_a, \sigma_s) = (\mu_a, 0)$  and other regions are pure scattering regions with  $(\sigma_a, \sigma_s) = (0, \mu_s)$ . A source term defined by

$$G(x, y) = \begin{cases} 1.0, & \text{if } |x - 2.5| < 0.5 \text{ and } |y - 2.5| < 0.5, \\ 0, & \text{otherwise,} \end{cases}$$

is imposed in the orange region at the center of the computational domain. The parameter for this problem  $\boldsymbol{\mu} = (\mu_a, \mu_s) \in [95, 105] \times [0.5, 1.5]$  determines the strength of absorption and scattering in the corresponding regions. We use an  $80 \times 80$  uniform mesh in space and CL(40, 6) angular discretization. A reference full order solution is presented in the right picture of Fig. 1. We set the tolerance for the relative residual in (F)GMRES solvers to  $10^{-11}$ .

The training set for this problem are 121 pairs of uniformly sampled  $(\mu_a, \mu_s)$  from  $[95, 105] \times [0.5, 1.5]$ . We select  $\boldsymbol{\mu}_1 = (100, 1)$  to start the greedy algorithm. We test the performance of our method with 10 pairs of randomly sampled parameters outside the training set.

**Online efficiency:** In Tab. 1, we present the results using ROMs constructed with  $\mathbf{w} = 2$  and various values of the tolerance  $\epsilon_{\text{ROM}}$ . Compared to GMRES-DSA, FGMRES-ROMSAD achieves comparable accuracy

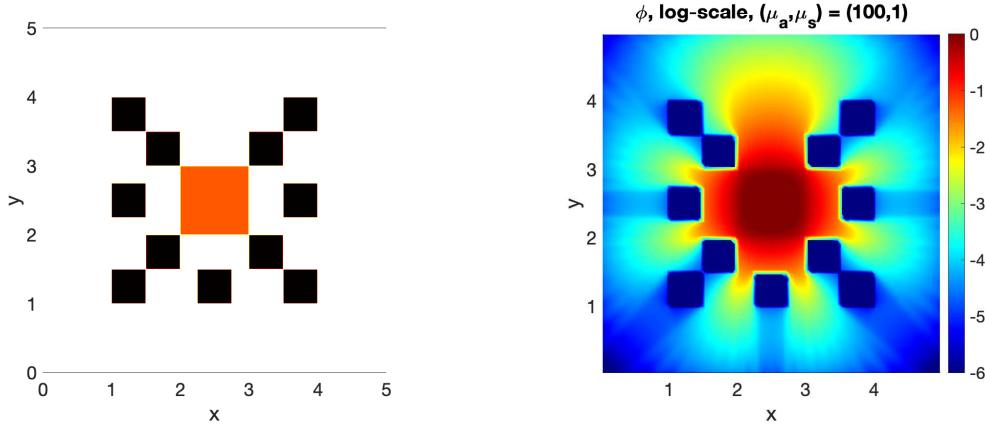


Figure 1: The set-up and a reference solution for the lattice problem in Sec. 5.1. Left: the set-up for the lattice problem. Black: pure absorption regions with  $(\sigma_a, \sigma_s) = (\mu_a, 0)$ . White and orange: pure scattering regions with  $(\sigma_a, \sigma_s) = (0, \mu_s)$ . Orange: constant source term with  $G = 1$ . Right: the reference solution under log-scale for  $(\mu_a, \mu_s) = (100, 1.0)$ . We want to point out that negative scalar flux can be generated in this example, but it will not break the linear solver, since we are not considering thermal radiation here. When generating the plot under log-scale, we take  $\max(10^{-16}, \phi(\mathbf{x}))$ .

and approximately 2.43 times acceleration with  $\epsilon_{\text{ROM}} = 10^{-7}$ , 2.61 times acceleration with  $\epsilon_{\text{ROM}} = 10^{-8}$  and 3.00 times acceleration with  $\epsilon_{\text{ROM}} = 10^{-9}$ . As expected, the smaller tolerance  $\epsilon_{\text{ROM}}$ , the greater acceleration is achieved. The average relative computational time is approximately proportional to the average number of transport sweeps needed for convergence.

	$\epsilon_{\text{ROM}}$	GMRES-DSA	FGMRES-ROMSAD
$\bar{n}_{\text{sweep}}$	$10^{-7}$	10.7	5.0
$T_{\text{rel}}$		100%	43.02%
$\mathcal{R}_{\infty}$		$1.01 \times 10^{-12}$	$1.49 \times 10^{-12}$
$\bar{n}_{\text{sweep}}$	$10^{-8}$	10.7	4.5
$T_{\text{rel}}$		100%	38.30%
$\mathcal{R}_{\infty}$		$1.01 \times 10^{-12}$	$1.50 \times 10^{-12}$
$\bar{n}_{\text{sweep}}$	$10^{-9}$	10.7	3.9
$T_{\text{rel}}$		100%	33.30%
$\mathcal{R}_{\infty}$		$1.01 \times 10^{-12}$	$1.55 \times 10^{-12}$

Table 1: Results for the lattice problem in Sec. 5.1 with the window size  $\mathfrak{w} = 2$ . Dimensions of the reduced order spaces:  $r = 34$  for  $\epsilon_{\text{ROM}} = 10^{-7}$ ;  $r = 44$  for  $\epsilon_{\text{ROM}} = 10^{-8}$ ;  $r = 50$  for  $\epsilon_{\text{ROM}} = 10^{-9}$ .

**Offline efficiency:** In Tab. 2, we present the offline computational times for various steps in the greedy algorithm, and compare the computational time of the greedy algorithm  $T_{\text{greedy}}$  and generating snapshots for all the 121 parameters in the training set  $T_{\text{All Snap.}}$ . The ratio  $T_{\text{All Snap.}}/T_{\text{greedy}}$  is approximately 4.06 with  $\epsilon_{\text{ROM}} = 10^{-7}$ , 3.37 with  $\epsilon_{\text{ROM}} = 10^{-8}$  and 3.04 with  $\epsilon_{\text{ROM}} = 10^{-9}$ , demonstrating the computational saving gained by applying the greedy algorithm. The lower the value of  $\epsilon_{\text{ROM}}$ , the more parameters are sampled, leading to the less saving gained offline, but the better efficiency online. Regardless of the value for  $\epsilon_{\text{ROM}}$ , the main computational cost in the greedy algorithm is consistently from the step 1 and the step 2(a), which are generating right-hand sides of the memory-efficient formulations for all training parameters and high-fidelity linear solves for sampled parameters, respectively.

$T_{\text{Step 1}}/T_{\text{greedy}}$	$T_{\text{Step 2(a)}}/T_{\text{greedy}}$	$T_{\text{Step 2(b)}}/T_{\text{greedy}}$	$T_{\text{Step 2(c)}}/T_{\text{greedy}}$	$T_{\text{Step 3}}/T_{\text{greedy}}$	$T_{\text{All Snap.}}/T_{\text{greedy}}$
30.55%	51.46%	8.84%	0.98%	8.17%	4.06

(a)  $\epsilon_{\text{ROM}} = 10^{-7}$ , 17 sampled parameters

$T_{\text{Step 1}}/T_{\text{greedy}}$	$T_{\text{Step 2(a)}}/T_{\text{greedy}}$	$T_{\text{Step 2(b)}}/T_{\text{greedy}}$	$T_{\text{Step 2(c)}}/T_{\text{greedy}}$	$T_{\text{Step 3}}/T_{\text{greedy}}$	$T_{\text{All Snap.}}/T_{\text{greedy}}$
25.31%	55.09%	9.50%	1.35%	8.75%	3.37

(b)  $\epsilon_{\text{ROM}} = 10^{-8}$ , 22 sampled parameters

$T_{\text{Step 1}}/T_{\text{greedy}}$	$T_{\text{Step 2(a)}}/T_{\text{greedy}}$	$T_{\text{Step 2(b)}}/T_{\text{greedy}}$	$T_{\text{Step 2(c)}}/T_{\text{greedy}}$	$T_{\text{Step 3}}/T_{\text{greedy}}$	$T_{\text{All Snap.}}/T_{\text{greedy}}$
22.89%	56.79%	9.77%	1.57%	8.98%	3.04

(c)  $\epsilon_{\text{ROM}} = 10^{-9}$ , 25 sampled parameters

Table 2: Offline results for the lattice problem in Sec. 5.1.  $T_{\text{greedy}}$ : the computational time of the greedy algorithm offline.  $T_{\text{Step } k}$ : the computational time of the  $k$ -th step in the greedy algorithm offline.  $T_{\text{All Snap.}}$ : the computational time of generating all the snapshots for the 121 parameters in the training set  $\mathcal{P}_{\text{train}}$ .

## 5.2. Pin-cell problem

We consider a parametric pin-cell problem with zero inflow boundary conditions and Gaussian source  $G(x, y) = \exp(-100(x^2 + y^2))$  on the computational domain  $\Gamma_{\mathbf{x}} = [-1, 1]^2$ . The setup is illustrated in the left picture of Fig. 2. The outer black region is defined as  $\{(x, y) : |x| > 0.5 \text{ or } |y| > 0.5\}$ , where only strong scattering effect ( $\sigma_s = 100$ ) exists. The inner white region, defined as  $\{(x, y) : |x| \leq 0.5 \text{ and } |y| \leq 0.5\}$ , has parametric scattering and absorption cross sections given by  $(\sigma_a, \sigma_s) = (\mu_a, \mu_s) \in [0.05, 0.5]^2$ . The scattering effect in the outer black region is 200 to 2000 times as strong as the scattering effect in the inner white region, leading to significant multiscale effects in this problem. We partition the computational domain with an  $80 \times 80$  uniform mesh and apply CL(30, 6) angular discretization. The tolerance for the relative residual of (F)GMRES is set to  $10^{-11}$ .

The training set for this problem consists of 25 uniformly sampled parameters from  $[0.05, 0.5]^2$ . The ROM is generated with the initial sample  $\boldsymbol{\mu}_1 = (0.275, 0.275)$ , a window size  $\mathbf{w} = 2$  and a tolerance of  $\epsilon_{\text{ROM}} = 10^{-10}$ . We test the performance of the ROMSAD preconditioner with 10 randomly sampled parameters outside the training set.

**Online efficiency:** As shown in Tab. 3, FGMRES-ROMSAD, on average, converges with 5.1 transport sweeps per parameter, and achieves approximately 3.33 times acceleration over GMRES-DSA.

**Comparison with SI-ROMSAD:** As presented in [35], for this pin-cell problem, SI-ROMSAD, whose underlying ROM is constructed using the POD method with data from all the 25 training parameters and a singular value decomposition (SVD) with truncation tolerance  $10^{-9}$ , achieves 10 times acceleration over SI-DSA and 4 times acceleration over GMRES with a left DSA preconditioner. Using such an accurate ROM, SI-ROMSAD is highly effective.

However, we will use the following setup to demonstrate that when the ROM is not highly accurate, FGMRES-ROMSAD is more robust than SI-ROMSAD. Since the corrections in the first iteration are the same for FGMRES and SI, up to a scaling factor, we set the window size  $\mathbf{w} = 1$  and  $\epsilon_{\text{ROM}} = 10^{-7}$  when building the ROM with the greedy algorithm. This ROM is employed in both FGMRES-ROMSAD and SI-ROMSAD, and we test their performance with the most challenging parameter for ROMSAD in our test set  $(\mu_a, \mu_s) = (0.065886, 0.11397)$ . The full order reference solution for this parameter is presented in the right picture of Fig. 2. Sharp features in the scalar flux can be observed near the material interface. The stopping criterion for SI is whether the absolute  $l_2$  residual  $\|\mathbf{r}^{(l)}\|_2 = \|\boldsymbol{\phi}^{(l,*)} - \boldsymbol{\phi}^{(l-1)}\|_2$  is smaller than  $10^{-11} \times \|\tilde{\mathbf{b}}\|_2$  with  $\tilde{\mathbf{b}}$  being the right hand side for the memory-efficient formulation.

As shown in Tab. 4, even with this relatively less accurate ROM, FGMRES-ROMSAD still achieves 1.33 times acceleration over GMRES-DSA and 4.71 times acceleration over SI-DSA. In contrast, SI-ROMSAD is unable to reach the desired accuracy within 100 iterations, while SI-DSA converges in 49 iterations. In both FGMRES-ROMSAD and SI-ROMSAD, DSA starts to be applied after the first SA correction. The relative



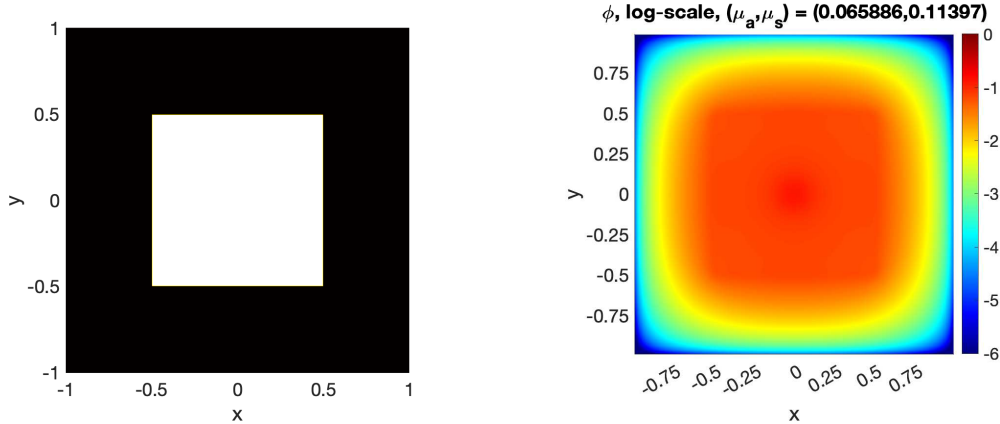


Figure 2: The set-up and reference solutions for the pin-cell problem in Sec. 5.2. Left: problem set-up. Right:  $\phi$  for  $(\mu_s, \mu_a) = (0.065886, 0.11397)$  (under log-scale).

$l_2$  residuals after the first correction of FGMRES-ROMSAD and SI-ROMSAD are comparable and much smaller than that of GMRES-DSA and SI-DSA, demonstrating the effectiveness of the ROM-based correction. However, despite using the same preconditioner from the second iteration and starting from a smaller relative residual, SI-ROMSAD surprisingly converges much more slowly than SI-DSA. We suspect that this slowdown is due to the robustness degeneration of SI-DSA for problems with discontinuous materials [17, 6].

**Offline efficiency:** The training set consists of a total of 25 parameters. In the offline stage, the greedy algorithm samples 22 parameters from this set. As shown in Tab. 5, the computational time of the greedy algorithm is nearly the same as generating high-fidelity snapshots for the entire training set. In summary, when the number of representative parameters is close to the size of the training set, the benefit in using the greedy offline algorithm is less pronounced.

	GMRES-DSA	FGMRES-ROMSAD
$\bar{n}_{\text{sweep}}$	15.5	5.1
$T_{\text{rel}}$	100%	30.05%
$\mathcal{R}_{\infty}$	$5.14 \times 10^{-13}$	$5.75 \times 10^{-13}$

Table 3: Online results for the pin-cell problem in Sec. 5.2. In the offline stage, 22 parameters are sampled, resulting in a reduced order space whose dimension is 44.

	GMRES-DSA	SI-DSA	FGMRES-ROMSAD	SI-ROMSAD
$n_{\text{sweep}}$	15	49	10	100 (★)
$T_{\text{rel}}$	100%	323.05%	68.55%	663.47%
$\mathcal{R}_{\infty}$	$7.72 \times 10^{-13}$	$4.35 \times 10^{-13}$	$2.20 \times 10^{-13}$	$1.18 \times 10^{-9}$
$\mathcal{R}_{\text{rel},2}$ after the first correction	$6.23 \times 10^{-2}$	$1.17 \times 10^{-1}$	$4.87 \times 10^{-6}$	$4.90 \times 10^{-6}$

Table 4: Comparison between FGMRES-ROMSAD and SI-ROMSAD for the pin-cell problem in Sec. 5.2 with  $(\mu_a, \mu_s) = (0.06589, 0.11397)$ . In the offline stage,  $\epsilon_{\text{ROM}} = 10^{-7}$ ,  $\mathbf{w} = 1$  and 13 parameters are sampled, resulting in a reduced order space whose dimension is 13.  $\mathcal{R}_{\text{rel},2}$ : relative  $l_2$  residual. ★: means that SI-ROMSAD fails to converge as its relative  $l_2$  residual almost gets stuck and decays very slowly.

$T_{\text{Step 1}}/T_{\text{greedy}}$	$T_{\text{Step 2(a)}}/T_{\text{greedy}}$	$T_{\text{Step 2(b)}}/T_{\text{greedy}}$	$T_{\text{Step 2(c)}}/T_{\text{greedy}}$	$T_{\text{Step 3}}/T_{\text{greedy}}$	$T_{\text{All Snap.}}/T_{\text{greedy}}$
5.08%	83.07%	9.40%	1.39%	1.04%	1.02

Table 5: Offline results for the pin-cell problem in Sec. 5.2.  $T_{\text{greedy}}$ : the computational time of the greedy algorithm offline.  $T_{\text{Step } k}$ : the computational time of the  $k$ -th step in the greedy algorithm offline.  $T_{\text{All Snap.}}$ : the computational time of generating all the snapshots for the 51 parameters in the training set  $\mathcal{P}_{\text{train}}$  using GMRES-DSA.

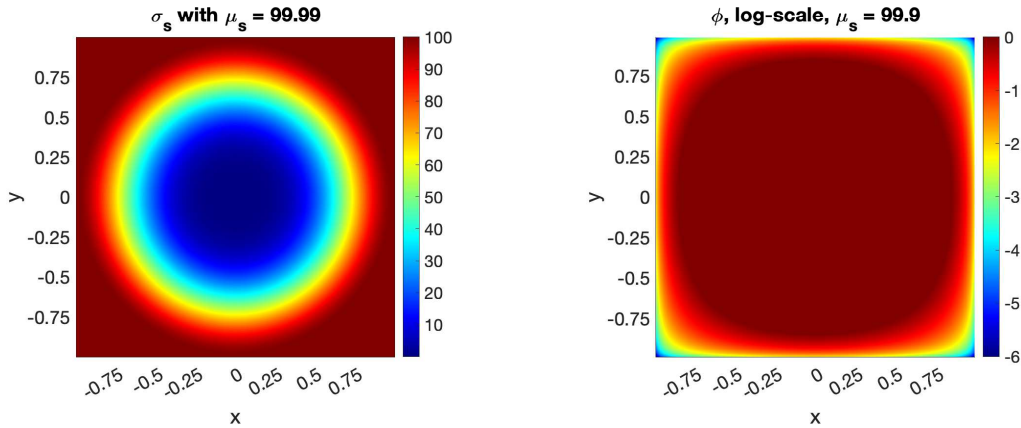


Figure 3: Left:  $\sigma_s(\mathbf{x})$  with  $\mu_s = 99.9$  for the variable scattering problem in Sec. 5.3. Right: corresponding angular flux.

### 5.3. Variable scattering problem

The final test involves a parametric variable scattering problem on the computational domain  $\Gamma_{\mathbf{x}} = [-1, 1]^2$ . The parametric scattering cross section is defined as

$$\sigma_s(x, y) = \begin{cases} \mu_s r^4 (2 - r^2)^2 + 0.1, & r = \sqrt{x^2 + y^2} \leq 1, \\ \mu_s + 0.1, & \text{otherwise,} \end{cases} \quad \mu_s \in [49.9, 99.9], \quad \sigma_a(x, y) = 0. \quad (39)$$

The scattering effect smoothly changes from 0.1 to  $\mu_s + 0.1 \in [50, 100]$  when moving from the center of the computational domain to its boundary. In other words, there is a smooth transition from transport dominant regime to scattering dominant regime in this problem. The parameter  $\mu_s$  determines the speed of this transition. The boundary condition is zero inflow boundary conditions. A Gaussian source  $G(x, y) = \frac{10}{\pi} \exp(-100(x^2 + y^2))$  is imposed within the computational domain. An  $80 \times 80$  uniform spatial mesh and  $\text{CL}(30, 6)$  angular discretization are applied. In Fig. 3, we present a configuration of the scattering cross section  $\sigma_s(\mathbf{x})$  and the corresponding high-fidelity reference solution.

The parameter of this problem,  $\mu_s \in [49.9, 99.9]$ , determines how quickly the scattering strength increases from the center to the boundary of the computational domain. We use a training set consisting of 51 uniformly sampled parameters, and set the initial sample, the window size and the tolerance in the greedy algorithm as  $\mu_{s,1} = 74.9$ ,  $\mathbf{w} = 2$  and  $\epsilon_{\text{ROM}} = 10^{-9}$ . The tolerance of relative residual for (F)GMRES solver is set to  $10^{-11}$ . We use 10 randomly sampled parameters outside the training set to test the performance of our ROMSAD preconditioner.

**Online efficiency:** In this example, we test the performance of ROMSAD coupled with different DSA preconditioners. Both the fully consistent (FC) and partially consistent (PC) DSA preconditioners are considered (see Appendix A for details).

As shown in Tab. 6, in GMRES-DSA, the right FC-DSA preconditioner results in a 26.67% reduction in the number of transport sweeps and 9.35% reduction in computational time compared to the right PC-DSA preconditioner. We suspect that the different percentage of the reduction in the number of transport sweeps and the computational time is due to the more computational cost required by FC-DSA in comparison

to PC-DSA. Conversely, by using ROM-based corrections in the first two iterations, FGMRES-ROMSAD converges in an average of 4.7 transport sweeps when using PC-DSA and 4.6 transport sweeps when using FC-DSA. Coupling ROM-based corrections with both FC-DSA and PC-DSA, FGMRES achieves at least 3.11 times acceleration over GMRES with PC-DSA preconditioner and 2.82 times acceleration over GMRES with FC-DSA preconditioner.

**Offline efficiency:** We observe that whether generating snapshots with the partially or fully consistent DSA preconditioner, the same parameters are sampled, and the difference between the resulting reduced order basis is negligible. Therefore, we present only the offline results with the fully consistent DSA in Tab. 7. The main cost of the greedy algorithm still comes from its step 1 and step 2(a), which are generating the right-hand sides for the memory-efficient formulation and the high fidelity solves for sampled parameters, respectively. Using the greedy algorithm to build the ROM only requires approximately 25.00% of the time needed to generate snapshots for all training parameters using GMRES with right FC-DSA preconditioner.

	GMRES-PC-DSA	GMRES-FC-DSA	FGMRES-PC-ROMSAD	FGMRES-FC-ROMSAD
$\bar{n}_{\text{sweep}}$	15.0	11.0	4.7	4.6
$T_{\text{rel}}$	100%	90.65%	30.61%	32.11%
$\mathcal{R}_{\infty}$	$9.26 \times 10^{-13}$	$3.22 \times 10^{-13}$	$1.05 \times 10^{-12}$	$5.32 \times 10^{-13}$

Table 6: Online results for the variable scattering problem in Sec. 5.3. In the offline stage, 8 parameters are sampled, resulting in a reduced order space whose dimension is 16. GMRES-PC/FC-DSA: GMRES with partially/fully consistent right DSA preconditioner. FGMRES-PC/FC-ROMSAD: FGMRES with ROMSAD preconditioner using partially/fully consistent DSA preconditioner. The relative computational cost is computed with respect to GMRES-PC-DSA.

$T_{\text{Step 1}}/T_{\text{greedy}}$	$T_{\text{Step 2(a)}}/T_{\text{greedy}}$	$T_{\text{Step 2(b)}}/T_{\text{greedy}}$	$T_{\text{Step 2(c)}}/T_{\text{greedy}}$	$T_{\text{Step 3}}/T_{\text{greedy}}$	$T_{\text{All Snap.}}/T_{\text{greedy}}$
26.08%	61.61%	8.51%	0.44%	3.3%	4.00

Table 7: Offline results for the variable scattering problem in Sec. 5.3.  $T_{\text{greedy}}$ : the computational time of the greedy algorithm offline.  $T_{\text{Step } k}$ : the computational time of the  $k$ -th step in the greedy algorithm offline.  $T_{\text{All Snap.}}$ : the computational time of generating all the snapshots for the 51 parameters in the training set  $\mathcal{P}_{\text{train}}$  using GMRES with right fully consistent DSA preconditioner.

## 6. Conclusions

In this paper, we extend the ROMSAD preconditioner from the SI framework to the Krylov framework and construct the underlying ROM more efficiently through a greedy algorithm.

From our numerical tests, we make the following observations.

1. In the online stage, FGMRES-ROMSAD outperforms GMRES with the right DSA preconditioner.
2. When the underlying ROM is not highly accurate, FGMRES-ROMSAD is more robust than SI-ROMSAD.
3. In the offline stage, if the number of representative parameters is much smaller than the size of the training set, the greedy algorithm can construct the ROM significantly more efficiently than methods that require high-fidelity data for the entire training set.

In the future, we aim to integrate the proposed method as a building block for multi-query applications such as uncertainty quantification, inverse problems and design optimization. Extensions to more complex problems involving multiple energy groups, highly peaked anisotropic scattering, and nonlinear thermal radiation are also of great interest.

## Acknowledgement

The author would like to thank Prof. Fengyan Li and from Rensselaer Polytechnic Institute and her student Kimberly Matsuda for their discussions, and reviewers of his previous work [35] for their interesting questions which motivates this paper.

## CRediT authorship contribution statement

**Zhichao Peng:** Writing – original draft, Writing – review & editing, Visualization, Validation, Software, Methodology, Data curation, Conceptualization.

## Declaration of generative AI and AI-assisted technologies in the writing process

During the preparation of this work the author(s) used ChatGPT in order to check grammar errors and improve readability. After using this tool/service, the author(s) reviewed and edited the content as needed and take(s) full responsibility for the content of the publication.

## Appendix A. Partially and fully consistent DSA

Following [5], we briefly outline how to derive a fully/partially consistent discretization for DSA. For simplicity, we consider 1D slab geometry with a angular discretization using a quadrature rule  $\{(\pm v_j, \omega_{\pm j})\}$  satisfying  $\omega_j = \omega_{-j}$ .

Let  $\{T_i = [x_{i-\frac{1}{2}}, x_{i+\frac{1}{2}}], i = 1, \dots, N_x\}$  be a partition of the computational domain and  $\{\eta_i(\mathbf{x})\}_{i=1}^{N_{\text{DOF}}}$  be an orthonormal basis for DG discrete space. We introduce the discrete advection operator with central flux  $\mathbf{D}_C \in \mathbb{R}^{N_{\text{DOF}} \times N_{\text{DOF}}}$  and the jump operator  $\mathbf{D}_J \in \mathbb{R}^{N_{\text{DOF}} \times N_{\text{DOF}}}$  as:

$$(\mathbf{D}_C)_{kl} = - \sum_{i=1}^{N_x} \left( \int_{T_i} \partial_x \eta_k(x) \eta_l(x) dx + \{\eta_l(x_{i+\frac{1}{2}})\} [\eta_k(x_{i+\frac{1}{2}})] \right), \quad (\mathbf{D}_J)_{kl} = - \sum_{i=1}^{N_x} [\eta_l(x_{i+\frac{1}{2}})] [\eta_k(x_{i+\frac{1}{2}})], \quad (\text{A.1a})$$

$$\{\eta_l(x_{i+\frac{1}{2}})\} = \left( \eta_l(x_{i+\frac{1}{2}}^+) + \eta_l(x_{i+\frac{1}{2}}^-) \right) / 2 \quad \text{and} \quad [\phi_k(x_{i+\frac{1}{2}})] = \eta_l(x_{i+\frac{1}{2}}^+) - \eta_l(x_{i+\frac{1}{2}}^-) \quad (\text{A.1b})$$

Then, the discrete upwind advection operator is  $\mathbf{D}_j = v_j \left( \mathbf{D}_C - \frac{\text{sign}(v_j)}{2} \mathbf{D}_J \right)$ .

Assume  $\delta\psi^{(l)}(x, v_j)$  can be represented as a  $P_1$  expansion  $\delta\psi^{(l)}(x, v_j) = \delta\phi^{(l)}(x) + 3v_j\delta J^{(l)}(x)$ , then we have the discrete correction equation:

$$\left( v_j (\mathbf{D}_C - \frac{1}{2} \mathbf{D}_J) + \boldsymbol{\Sigma}_t \right) \left( \delta\phi^{(l)} + 3v_j \delta J^{(l)} \right) = \boldsymbol{\Sigma}_s \delta\phi + \boldsymbol{\Sigma}_s (\phi^{(l,*)} - \phi^{(l-1)}), \quad \text{if } v_j \geq 0, \quad (\text{A.2a})$$

$$\left( v_j (\mathbf{D}_C + \frac{1}{2} \mathbf{D}_J) + \boldsymbol{\Sigma}_t \right) \left( \delta\phi^{(l)} + 3v_j \delta J^{(l)} \right) = \boldsymbol{\Sigma}_s \delta\phi + \boldsymbol{\Sigma}_s (\phi^{(l,*)} - \phi^{(l-1)}), \quad \text{if } v_j < 0. \quad (\text{A.2b})$$

Taking the discrete zero-th and first order moment of (A.2) in the angular space, we obtain

$$\mathbf{D}_C \delta \mathbf{J}^{(l)} - \left( \sum_{v_j > 0} \omega_j v_j \right) \mathbf{D}_J \delta \boldsymbol{\rho}^{(l)} + \boldsymbol{\Sigma}_a \delta \boldsymbol{\phi}^{(l)} = \boldsymbol{\Sigma}_s (\boldsymbol{\phi}^{(l,*)} - \boldsymbol{\rho}^{(l-1)}), \quad (\text{A.3a})$$

$$\left( \sum_{j=1}^{N_v} \omega_j v_j^2 \right) \mathbf{D}_C \delta \boldsymbol{\phi}^{(l)} + \left( \boldsymbol{\Sigma}_t - 3 \left( \sum_{v_j > 0} \omega_j v_j^3 \right) \mathbf{D}_J \right) \delta \mathbf{J}^{(l)} = 0. \quad (\text{A.3b})$$

Equation (A.3b) yields

$$\delta \mathbf{J}^{(l)} = - \left( \sum_{j=1}^{N_v} \omega_j v_j^2 \right) \left( \boldsymbol{\Sigma}_t - 3 \left( \sum_{v_j > 0} \omega_j v_j^3 \right) \mathbf{D}_J \right)^{-1} \mathbf{D}_C \delta \boldsymbol{\rho}^{(l)}. \quad (\text{A.4})$$

Substituting (A.4) into (A.3a) to eliminate  $\delta \mathbf{J}^{(l)}$ , we obtain a fully consistent DSA. If dropping the  $\mathbf{D}_J$  term in (A.4) before substituting it into (A.3a), we obtain the partially consistent DSA in [11].

## References

- [1] S. R. Arridge, J. C. Schotland, Optical tomography: forward and inverse problems, *Inverse problems* 25 (12) (2009) 123010.
- [2] R. Spurr, T. Kurosu, K. Chance, A linearized discrete ordinate radiative transfer model for atmospheric remote-sensing retrieval, *Journal of Quantitative Spectroscopy and Radiative Transfer* 68 (6) (2001) 689–735.
- [3] G. C. Pomraning, *The equations of radiation hydrodynamics*, International Series of Monographs in Natural Philosophy, Oxford: Pergamon Press (1973).
- [4] H.-T. Janka, K. Langanke, A. Marek, G. Martínez-Pinedo, B. Müller, Theory of core-collapse supernovae, *Physics Reports* 442 (1-6) (2007) 38–74.
- [5] M. L. Adams, Discontinuous finite element transport solutions in thick diffusive problems, *Nuclear science and engineering* 137 (3) (2001) 298–333.
- [6] J. S. Warsa, T. A. Wareing, J. E. Morel, Krylov iterative methods and the degraded effectiveness of diffusion synthetic acceleration for multidimensional SN calculations in problems with material discontinuities, *Nuclear science and engineering* 147 (3) (2004) 218–248.
- [7] Y. Azmy, E. Sartori, E. W. Larsen, J. E. Morel, Advances in discrete-ordinates methodology, *Nuclear computational science: A century in review* (2010) 1–84.
- [8] H. Kopp, Synthetic method solution of the transport equation, *Nuclear Science and Engineering* 17 (1) (1963) 65–74.
- [9] R. Alcouffe, Diffusion Synthetic Acceleration Methods For the Diamond-Differenced Discrete-Ordinates Equations, *Nuclear science and engineering* 64 (1977) 344–355.
- [10] M. L. Adams, W. R. Martin, Diffusion synthetic acceleration of discontinuous finite element transport iterations, *Nuclear science and engineering* 111 (2) (1992) 145–167.
- [11] T. Wareing, New diffusion-synthetic acceleration methods for the  $S_N$  equations with corner balance spatial differencing (1993).
- [12] M. L. Adams, E. W. Larsen, Fast iterative methods for discrete-ordinates particle transport calculations, *Progress in Nuclear Energy* 40 (2002) 3–159.
- [13] V. Y. Gol’din, A quasi-diffusion method of solving the kinetic equation, *Zhurnal Vychislitel’noi Matematiki i Matematicheskoi Fiziki* 4 (6) (1964) 1078–1087.
- [14] D. Y. Anistratov, V. Y. Gol’Din, Nonlinear methods for solving particle transport problems, *Transport Theory and Statistical Physics* 22 (2-3) (1993) 125–163.
- [15] S. Olivier, W. Pazner, T. S. Haut, B. C. Yee, A family of independent Variable Eddington Factor methods with efficient preconditioned iterative solvers, *Journal of Computational Physics* 473 (2023) 111747.
- [16] L. J. Lorence Jr, J. Morel, E. W. Larsen, An  $S_2$  synthetic acceleration scheme for the one-dimensional sn equations with linear discontinuous spatial differencing, *Nuclear Science and Engineering* 101 (4) (1989) 341–351.
- [17] Y. Azmy, Unconditionally stable and robust adjacent-cell diffusive preconditioning of weighted-difference particle transport methods is impossible, *Journal of Computational Physics* 182 (1) (2002) 213–233.
- [18] K. Ren, R. Zhang, Y. Zhong, A fast algorithm for radiative transport in isotropic media, *Journal of Computational Physics* 399 (2019) 108958.

- [19] P. Benner, S. Gugercin, K. Willcox, A survey of projection-based model reduction methods for parametric dynamical systems, *SIAM review* 57 (4) (2015) 483–531.
- [20] A. G. Buchan, A. Calloo, M. G. Goffin, S. Dargaville, F. Fang, C. C. Pain, I. M. Navon, A POD reduced order model for resolving angular direction in neutron/photon transport problems, *Journal of Computational Physics* 296 (2015) 138–157.
- [21] J. Tencer, K. Carlberg, M. Larsen, R. Hogan, Accelerated solution of discrete ordinates approximation to the boltzmann transport equation for a gray absorbing–emitting medium via model reduction, *Journal of Heat Transfer* 139 (12) (2017) 122701.
- [22] Y. Choi, P. Brown, W. Arrighi, R. Anderson, K. Huynh, Space–time reduced order model for large-scale linear dynamical systems with application to boltzmann transport problems, *Journal of Computational Physics* 424 (2021) 109845.
- [23] M. Tano, J. Ragusa, D. Caron, P. Behne, Affine reduced-order model for radiation transport problems in cylindrical coordinates, *Annals of Nuclear Energy* 158 (2021) 108214.
- [24] P. Behne, J. Vermaak, J. C. Ragusa, Minimally-invasive parametric model-order reduction for sweep-based radiation transport, *Journal of Computational Physics* 469 (2022) 111525.
- [25] P. Behne, J. Vermaak, J. Ragusa, Parametric Model-Order Reduction for Radiation Transport Simulations Based on an Affine Decomposition of the Operators, *Nuclear Science and Engineering* 197 (2) (2023) 233–261.
- [26] I. Halvic, J. C. Ragusa, Non-intrusive model order reduction for parametric radiation transport simulations, *J. Comput. Phys.* 492 (2023) 112385.
- [27] R. G. McClarren, T. S. Haut, Data-driven acceleration of thermal radiation transfer calculations with the dynamic mode decomposition and a sequential singular value decomposition, *Journal of Computational Physics* 448 (2022) 110756.
- [28] Z. Peng, Y. Chen, Y. Cheng, F. Li, A reduced basis method for radiative transfer equation, *Journal of Scientific Computing* 91 (1) (2022) 1–27.
- [29] J. M. Coale, D. Y. Anistratov, Reduced order models for thermal radiative transfer problems based on moment equations and data-driven approximations of the Eddington tensor, *Journal of Quantitative Spectroscopy and Radiative Transfer* 296 (2023) 108458.
- [30] J. M. Coale, D. Y. Anistratov, A reduced-order model for nonlinear radiative transfer problems based on moment equations and POD-Petrov-Galerkin projection of the normalized Boltzmann transport equation, *J. Comput. Phys.* 509 (2024) 113044.
- [31] Z. Peng, Y. Chen, Y. Cheng, F. Li, A micro-macro decomposed reduced basis method for the time-dependent radiative transfer equation, *Multiscale Model. Simul.* 22 (1) (2024) 639–666.
- [32] A. G. Buchan, I. M. Navon, L. Yang, A reduced order model discretisation of the space-angle phase-space dimensions of the Boltzmann transport equation with application to nuclear reactor problems, *J. Comput. Phys.* 517 (2024) 113268.
- [33] Z. K. Hardy, J. E. Morel, Proper Orthogonal Decomposition Mode Coefficient Interpolation: A Non-Intrusive Reduced-Order Model for Parametric Reactor Kinetics, *Nucl. Sci. Eng.* 198 (4) (2024) 832–852.
- [34] K. Matsuda, Y. Chen, Y. Cheng, F. Li, Reduced basis methods for parametric steady-state radiative transfer equation, paper under preparation.

- [35] Z. Peng, Reduced order model enhanced source iteration with synthetic acceleration for parametric radiative transfer equation, *Journal of Computational Physics* 517 (2024) 113303.
- [36] J. S. Hesthaven, G. Rozza, B. Stamm, et al., *Certified reduced basis methods for parametrized partial differential equations*, Vol. 590, Springer, 2016.
- [37] Y. Saad, A flexible inner-outer preconditioned GMRES algorithm, *SIAM Journal on Scientific Computing* 14 (2) (1993) 461–469.
- [38] R. G. McClarren, Calculating time eigenvalues of the neutron transport equation with dynamic mode decomposition, *Nuclear Science and Engineering* 193 (8) (2019) 854–867.
- [39] J. A. Roberts, L. Xu, R. Elzohery, M. Abdo, Acceleration of the power method with dynamic mode decomposition, *Nucl. Sci. Eng.* 193 (12) (2019) 1371–1378.
- [40] E. Smith, I. Variansyah, R. McClarren, Variable dynamic mode decomposition for estimating time eigenvalues in nuclear systems, *Nucl. Sci. Eng.* 197 (8) (2023) 1769–1778.
- [41] M. E. Tano, J. C. Ragusa, Sweep-net: an artificial neural network for radiation transport solves, *Journal of Computational Physics* 426 (2021) 109757.
- [42] K. Chen, Q. Li, J. Lu, S. J. Wright, A Low-Rank Schwarz Method for Radiative Transfer Equation With Heterogeneous Scattering Coefficient, *Multiscale Modeling & Simulation* 19 (2) (2021) 775–801.
- [43] W. Dahmen, F. Gruber, O. Mula, An adaptive nested source term iteration for radiative transfer equations, *Math. Comput.* 89 (324) (2020) 1605–1646.
- [44] J. Fu, M. Tang, A fast offline/online forward solver for stationary transport equation with multiple inflow boundary conditions and varying coefficients, *arXiv preprint arXiv:2401.03147* (2024).
- [45] Q. Song, J. Fu, M. Tang, L. Zhang, An Adaptive Angular Aomain Compression Scheme For Solving Multiscale Radiative Transfer Equation, *arXiv preprint arXiv:2408.08783* (2024).
- [46] Z. Peng, R. G. McClarren, M. Frank, A low-rank method for two-dimensional time-dependent radiation transport calculations, *Journal of Computational Physics* 421 (2020) 109735.
- [47] L. Einkemmer, J. Hu, Y. Wang, An asymptotic-preserving dynamical low-rank method for the multi-scale multi-dimensional linear transport equation, *Journal of Computational Physics* 439 (2021) 110353.
- [48] Z. Peng, R. G. McClarren, A high-order/low-order (HOLO) algorithm for preserving conservation in time-dependent low-rank transport calculations, *Journal of Computational Physics* 447 (2021) 110672.
- [49] J. Kusch, P. Stammer, A robust collision source method for rank adaptive dynamical low-rank approximation in radiation therapy, *arXiv preprint arXiv:2111.07160* (2021).
- [50] P. Yin, E. Endeve, C. Hauck, S. Schnake, Towards dynamical low-rank approximation for neutrino kinetic equations. Part I: Analysis of an idealized relaxation model, *Math. Comput.* (2024).
- [51] L. Einkemmer, J. Hu, J. Kusch, Asymptotic-Preserving and Energy Stable Dynamical Low-Rank Approximation, *SIAM Journal on Numerical Analysis* 62 (1) (2024) 73–92.
- [52] W. A. Sands, W. Guo, J.-M. Qiu, T. Xiong, High-order Adaptive Rank Integrators for Multi-scale Linear Kinetic Transport Equations in the Hierarchical Tucker Format, *arXiv:2406.19479* (2024).
- [53] M. Bachmayr, R. Bardin, M. Schlottbom, Low-rank tensor product Richardson iteration for radiative transfer in plane-parallel geometry, *arXiv:2403.14229* (2024).

- [54] D. Pasetto, M. Ferronato, M. Putti, A reduced order model-based preconditioner for the efficient solution of transient diffusion equations, *Int. J. Numer. Methods Eng.* 109 (8) (2017) 1159–1179.
- [55] N. D. Santo, S. Deparis, A. Manzoni, A. Quarteroni, Multi space reduced basis preconditioners for large-scale parametrized PDEs, *SIAM Journal on Scientific Computing* 40 (2) (2018) A954–A983.
- [56] G. D. Cortes, C. Vuik, J. D. Jansen, On POD-based deflation vectors for DPCG applied to porous media problems, *Journal of Computational and Applied Mathematics* 330 (2018) 193–213.
- [57] G. B. Diaz Cortés, C. Vuik, J.-D. Jansen, Accelerating the solution of linear systems appearing in two-phase reservoir simulation by the use of pod-based deflation methods, *Comput. Geosci* 25 (5) (2021) 1621–1645.
- [58] S. Hou, Y. Chen, Y. Xia, A reduced basis warm-start iterative solver for the parameterized linear systems, *arXiv preprint arXiv:2311.13862* (2023).
- [59] S. Jin, Asymptotic preserving (AP) schemes for multiscale kinetic and hyperbolic equations: a review, *Lecture notes for summer school on methods and models of kinetic theory (M&MKT), Porto Ercole (Grosseto, Italy)* (2010) 177–216.
- [60] J.-L. Guermond, G. Kanschat, Asymptotic analysis of upwind discontinuous Galerkin approximation of the radiative transport equation in the diffusive limit, *SIAM Journal on Numerical Analysis* 48 (1) (2010) 53–78.
- [61] Y. Saad, M. H. Schultz, GMRES: A generalized minimal residual algorithm for solving nonsymmetric linear systems, *SIAM Journal on scientific and statistical computing* 7 (3) (1986) 856–869.
- [62] M. Barrault, Y. Maday, N. C. Nguyen, A. T. Patera, An ‘empirical interpolation’ method: application to efficient reduced-basis discretization of partial differential equations, *Comptes Rendus Mathématique* 339 (9) (2004) 667–672.
- [63] S. Chaturantabut, D. C. Sorensen, Nonlinear model reduction via discrete empirical interpolation, *SIAM Journal on Scientific Computing* 32 (5) (2010) 2737–2764.
- [64] L. Chen, *iFEM: an integrated finite element methods package in MATLAB*, Tech. rep. (2009).  
URL <https://github.com/lyc102/ifem>